

Cosmological tests of the gravastar hypothesis

K. A. S. CROKER

Department of Physics & Astronomy, University of Hawai'i at Mānoa, 2505 Correa Rd., Honolulu, Hawai'i 96822, USA

(Dated: September 3, 2017)

ABSTRACT

Gravitational vacuum stars (gravastars) have become a viable theoretical alternative to the black hole (BH) end-stage of stellar evolution. These objects gravitate in vacuum like BHs, yet have no event horizons. In this paper, we present tests of the gravastar hypothesis within flat Friedmann cosmology. Such tests are complementary to optical and gravitational wave merger signatures, which have uncertainties dominated by the poorly constrained gravastar crust. We motivate our analysis directly from the action principle, and show that a population of gravastars must induce a time-dependent dark energy (DE). The possibility of such a contribution has been overlooked due to a subtlety in the *de facto* definition of the isotropic and homogeneous stress. Conservation of stress-energy directly relates the time evolution of this DE contribution to the measured BH comoving mass function and a gravastar population crust parameter η . We show that a population of gravastars formed between redshift $8 \lesssim z \lesssim 20$ readily produces the present-day DE density over a large range of η , providing a natural resolution to the coincidence problem. We compute an effective DE equation of state $w_{\text{eff}}(a)$ as a function of present-epoch BH population observables and η . Using a BH population model developed from the cosmic star formation history, we obtain w_0 and w_a consistent with Planck best-fit values. In summary, the gravastar hypothesis leads to an unexpected correlation between the BH population and the magnitude and time-evolution of DE.

Keywords: dark energy, stars: black holes

arXiv:1612.07245v3 [astro-ph.CO] 3 Sep 2017

1. INTRODUCTION

The recent direct observation of gravitational radiation from ultracompact, massive, object mergers provides definitive proof of the existence of objects with exterior geometries consistent with the classical black hole (BH) solutions. Unfortunately, the various boundaries and interiors of the classical BH geometries are severely pathological. In fact, the predicted physical curvature singularities and closed timelike curves had already motivated the exploration of BH “mimickers.” Such solutions to classical GR appear as classical BH geometries, as perceived by exterior vacuum observers, but replace the interior with another GR solution. Gliner (1966) is usually recognized as the first researcher to suggest that “ μ vacuum,” localized regions of vacuum with large cosmological constant, could be relevant during gravitational collapse.

A simplified scenario, which motivates more physically plausible constructions, is the following exact, spherically symmetric, GR solution

$$ds^2 = -\beta dt^2 + \beta^{-1} dr^2 + r^2 [d\theta^2 + \sin^2 \theta d\phi^2] \quad (1)$$

with

$$\beta(r) \equiv \begin{cases} 1 - (r/2M)^2 & r \leq 2M \\ 1 - 2M/r & r > 2M. \end{cases} \quad (2)$$

This solution is a Schwarzschild BH exterior for $r > 2M$, and a vacuum with cosmological constant interior to $r < 2M$. This solution is static, consistent with the intuition that material under tension stays bound. Note that the interior energy density correctly integrates to M . This means that a *vacuum* observer at infinity will perceive a point mass M . The interior region contains no physical singularity, but the infinite pressure gradient at $r = 2M$ in Eqn. (1) suggests consideration of slightly more sophisticated GR solutions.

Dymnikova (1992, Eqn. (14)) produced a “G-lump” model without an infinite pressure gradient. About a decade later, Mazur & Mottola (2004) and Chapline (2003) proposed additional realizations of what is now called a gravitational vacuum star (gravastar). The essential feature of viable gravastars is a “crust” region of finite thickness slightly beyond $r = 2M$, which surrounds the de Sitter core. These objects have no trapped surface: each interior is in causal contact with the outside universe. In fact, this ability to resolve the BH information paradox sparked renewed interest in BH mimickers during the “firewall” debates initiated by Almheiri et al. (2013). Theoretical checks on gravastar stability to perturbations (e.g. Visser & Wiltshire 2004; Lobo 2006; DeBenedictis et al. 2006) and stability to rotation (e.g. Chirenti & Rezzolla 2008; Uchikata & Yoshida 2015; Maggio et al. 2017) have found large ranges of viable parameters describing the crust. Phenomenological checks from distinct

merger ringdown signatures, such as an altered quasinormal mode spectrum (e.g. Chirenti & Rezzolla 2007) have been computed. In addition, possible optical signatures from the crust itself (e.g. Broderick & Narayan 2007), accretion disks (e.g. Harko et al. 2009), and even direct lensing (Sakai et al. 2014) have been investigated.

The first direct detection of gravitational radiation from massive compact object mergers has greatly stimulated critical analysis of the gravastar scenario. Bhagwat et al. (2016, 2017) show that the existing aLIGO interferometer and the proposed Cosmic Explorer and Einstein telescopes can resolve the higher harmonics, which could probe the existence of gravastars. On the other hand, Chirenti & Rezzolla (2016) have already claimed, using the ringdown, that GW150914 likely did not result in a gravastar final state. Yunes et al. (2016) criticize the Chirenti & Rezzolla (2016) claim as premature, yet argue that ringdown decay faster than the light crossing time of the remnant poses the more severe challenge.

In all phenomenology to date, however, gravastar signatures depend critically on the unknown properties of the crust. In this paper, we address this problem and develop complementary observational signatures dominated instead by the known properties of the core. Before proceeding, we first comment on consistency with Birkhoff’s theorem, which gravitationally decouples the interior properties of a localized object from its surroundings. A necessary condition for Birkhoff’s theorem is vacuum boundary conditions. Thus, we will consider gravastars within Friedmann cosmology, which is nowhere vacuum.

Consistent with the theoretical motivation to resolve the BH information paradox, we will replace all BHs with gravastars. The following falsifiable experimental prediction for the physical dark energy (DE) density $\Omega_\Lambda^{\text{eff}}$

$$\kappa(a, a_c) \equiv \frac{1}{a^3} \exp\left(3 \int_{a_c}^a \frac{\eta(a')}{a'} da'\right) \quad (3)$$

$$\Omega_\Lambda^{\text{eff}}(a) = \frac{1}{a^3 \kappa(a)} \int_0^a \frac{d\Delta_{\text{BH}}}{da'} \kappa(a') da' \quad (4)$$

will then be obtained. Here η is a small parameter which measures the deviation of the gravastar contribution from pure de Sitter due to crusts, a_c is a cutoff before which there are no gravastars, and Δ_{BH} is the comoving BH density, which has just begun to be constrained by aLIGO. As detailed by Dwyer et al. (2015), the proposed Cosmic Explorer interferometer will be able to definitively constrain $\Delta_{\text{BH}}(a)$ with $\sim 10^5$ events per year, and out to redshift $z \sim 10$. The schematic gravastar given in Eqn. (1) has no crust, so $\eta \equiv 0$ and the prediction becomes entirely parameter-free

$$\Omega_\Lambda^{\text{eff}}(a) = \int_0^a \frac{d\Delta_{\text{BH}}}{da'} \frac{1}{a'^3} da'. \quad (5)$$

The rest of this paper is organized as follows. In §2, we motivate a departure from the *de facto* Friedmann source (DFFS). We then define notation that simplifies our calculations and clarifies the physical observables. In §3, we construct the appropriate cosmological source from an assumed population of gravastars. In §3.1, we produce the fundamental quantitative prediction relating the DE density to the observed BH population and the gravastar crust parameter η . In §4, we proceed chronologically through the history of the Universe and consider the influence of a gravastar population at three different epochs. In §4.1, we consider the formation of primordial gravastars and essentially exclude their production. In §4.2, we demonstrate that stellar processes between redshift $8 < z < 20$ can produce enough gravastars to account for the present-day DE density. In §4.3, we analyze the gravastar-induced DE at late times ($z < 5$) in the dark fluid framework described in Ade et al. (2016). Here, we produce predictions for the DE equation of state parameters w_0 and w_a in terms of present-day BH population observables.

A comprehensive set of appendices presents material complementary to the phenomenological results of this paper. Appendix A highlights non-trivial assumptions fundamental to the DFFS. Appendix B clarifies the spatially-averaged nature of the Friedmann source by deriving Friedmann’s equations directly from the principle of stationary action. Appendix C establishes that the positive pressure contributions of typical astrophysical systems can be ignored. Appendix D discusses how causality is maintained, given a non-trivial time dependence in the background cosmological source. Appendix E develops a simple model for the BH population in terms of the stellar population. Appendix F gives an upper bound for the pressures of large, virialized systems like clusters.

Except within the appendices, we take the time unit as the reciprocal present-day Hubble constant H_0^{-1} , the density unit as the critical density today ρ_{cr} , and set the speed of light $c \equiv 1$. For efficiency, we will often describe quantities with scale factor or redshift dependence as time-dependent. We will also freely use either scale factor a or redshift z , depending on which produces the more compact quantitative expression. Though we replace all BHs with gravastars, for consistency with existing astrophysical literature, we will often refer to these objects as BHs.

2. ISOTROPIC AND HOMOGENEOUS STRESS IN FRIEDMANN COSMOLOGY

Given the symmetries of the RW metric, RW observers cannot distinguish points: in a homogeneous and isotropic universe, every point is observationally identical. In other words, a RW universe does not contain any notion of interior or exterior. Perhaps surprisingly, the *de facto* Friedmann source (DFFS) implicitly violates homogeneity and isotropy.

As detailed in Appendix A, the DFFS assumes the ability to define a notion of interior and exterior, distinct for every mass distribution. This assumption is used to reduce spatially extended systems to effective point masses. These point masses are then considered to contribute only as a pressure-free “dust.”

Consistency, however, requires that the source to Einstein’s equations exhibit the same symmetries as the metric. This requirement holds at each order in a perturbative expansion of Einstein’s equations. In particular, the spatially uniform background source in Friedmann cosmology cannot contain any implicit notion of interior or exterior. In Appendix B, we construct a consistent Friedmann source (CFS) by application of the principle of stationary action to an inhomogeneous fluid ansatz. The resulting zero-order source simply becomes a flat spatial average.

In contrast to the DFFS, the spatial average present within the CFS necessarily incorporates *all* pressures: cluster interiors, stellar interiors and, should they exist, gravastar interiors. In Appendix C, we show that accounting for positive astrophysical pressure contributions makes no observable changes. The effect of any *negative* pressure contributions, however, can critically influence the background expansion. An averaged gravastar interior contribution is both negative and strong, with $|\mathcal{P}_s| \sim \rho_s$. This feature of gravastars ultimately leads to the unexpected and quantitative relation between the expansion rate and the BH population.

2.1. Two-component approximation

Let barred variables represent physical, as opposed to comoving, background quantities. We investigate the CFS with two contributions. The first contribution, the s -contribution, is an approximation to the influence of gravitationally bound systems with pressure

$$T_v^s \equiv -\bar{\rho}_s(a)\delta_0^\mu\delta_v^0 + \bar{\mathcal{P}}_s(a)\delta_i^\mu\delta_v^i. \quad (6)$$

It is an approximation because we do not attempt to track all pressures within the universe. For the primary discussion of this work, the s -contribution will be exclusively from gravastars. For the discussion in Appendix C, justifying why this is an excellent approximation, the s -contribution will be a severe upper-bound on positive pressure contributions from typical astrophysical systems.

As is well known, the constituents of tightly bound gravitational systems decouple from the expansion. The number density of these systems then dilutes with the physical volume. This behavior motivates the following definitions

$$\rho_s(a) \equiv \bar{\rho}_s(a)a^3 \quad (7)$$

$$\mathcal{P}_s(a) \equiv \bar{\mathcal{P}}_s(a)a^3 \quad (8)$$

allowing us to rewrite Eqn. (6) in an entirely equivalent way

$$T_v^\mu \equiv -\frac{\rho_s(a)}{a^3} \delta_0^\mu \delta_v^0 + \frac{\mathcal{P}_s(a)}{a^3} \delta_i^\mu \delta_v^i. \quad (9)$$

The explicit appearance of a^3 factors and time-dependent comoving quantities greatly simplifies many computations and will help to emphasize the difference between the DFFS and the CFS.

The second contribution, the 0-contribution, comes from collisionless matter

$$T_v^\mu \equiv -\frac{\rho_0(a)}{a^3} \delta_0^\mu \delta_v^0, \quad (10)$$

and is identical to the analogous term of the DFFS whenever $d\rho_0/da = 0$. This derivative statement is an example of the utility of time-dependent comoving densities, when highlighting the differences between the DFFS and the CFS.

In the gravastar scenario, effectively collisionless matter is processed into localized regions of de Sitter space. We thus populate $\rho_s(a)$ by depleting an appropriate fraction $\Delta(a)$ of the collisionless contribution

$$\rho_0(a) \equiv \Omega_m [1 - \Delta(a)]. \quad (11)$$

Here Ω_m is the observed matter fraction today. The depletion fraction $\Delta(a)$ is determined through astrophysical observation.

The CFS does not conserve particle number by construction, but this is not required by Einstein's equations (Weinberg 1972, §2.10). Covariant conservation of energy and momentum

$$\nabla_\mu \left[T_v^\mu + T_v^s \right] = 0, \quad (12)$$

however, necessarily populates both $\rho_s(a)$ and $\mathcal{P}_s(a)$ in a manner consistent with Einstein's equations. Thus, time-dependence in comoving $\rho_0(a)$, $\rho_s(a)$, and $\mathcal{P}_s(a)$ does not violate thermodynamics or energy conservation. For a discussion of causality in the context of a non-trivially time-dependent background, we direct the reader to Appendix D.

3. GRAVASTAR CONTRIBUTION TO THE FRIEDMANN EQUATIONS

A dynamically stable gravastar, with physically plausible structure, is more sophisticated than Eqns. (1) and (2). Both Dymnikova (1992) and Mazur & Mottola (2004) introduce a transition region, which ultimately encloses a dark energy interior. The possible nature of this ‘‘crust’’ has been studied extensively by Visser & Wiltshire (2004); Martin-Moruno et al. (2012) and others. There is consensus that substantial freedom exists in the construction of gravastar models. This freedom, while constrained, permits a range of crust thicknesses and equations of state. We will consider the following structure

- $r \leq 2M$: de Sitter interior
- $2M < r \leq 2M + \ell$: crust region
- $r > 2M + \ell$: vacuum exterior

where M is a gravastar mass and ℓ is a crust thickness. Note that we have simplified the model by placing the inner radius at the Schwarzschild radius. In any physical gravastar, this inner radius must be slightly beyond the Schwarzschild radius: this prevents the formation of a trapped surface. For our purposes, this nuance will not matter. The cosmological contribution from a plausible gravastar population thus consists of two components

$$\rho_s \equiv \rho_{\text{int}} + \rho_{\text{crust}} \quad (13)$$

$$\mathcal{P}_s \equiv -\rho_{\text{int}} + \mathcal{P}_{\text{crust}}. \quad (14)$$

Note that ρ_{int} , ρ_{crust} , and $\mathcal{P}_{\text{crust}}$ are not independent degrees of freedom because each gravastar has a model-dependent internal structure.

We may define an equation of state for the gravastar source

$$w_s \equiv \frac{-\rho_{\text{int}} + \mathcal{P}_{\text{crust}}}{\rho_{\text{int}} + \rho_{\text{crust}}}. \quad (15)$$

Mazur & Mottola (2004) assert that most of the energy density is expected to reside within each core and that $\mathcal{P} \sim \rho$ within each crust. It is thus reasonable to expand the aggregate quantities and discard higher-order terms

$$w_s = -1 + \frac{\mathcal{P}_{\text{crust}}}{\rho_{\text{int}}} \left(1 - \frac{\rho_{\text{crust}}}{\rho_{\text{int}}} + \dots \right) \quad (16)$$

$$\simeq -1 + \frac{\mathcal{P}_{\text{crust}}}{\rho_{\text{int}}}. \quad (17)$$

This expression successfully isolates ignorance of the crust to a small dimensionless parameter, which we now define as

$$\eta(a) \equiv \frac{\mathcal{P}_{\text{crust}}}{\rho_{\text{int}}}. \quad (18)$$

To avoid confusion, we emphasize now that w_s is not the Dark Energy equation of state as constrained by Planck. The relation between these two quantities will be explored thoroughly in §4.3.

3.1. Relation of ρ_s to the BH population

Let Δ_{BH} be the comoving coordinate BH mass density. The formation of gravastars, and any subsequent accretion, depletes the baryon population. This decreases ρ_0 by Δ_{BH} as per Eqn (11). Consistent with the results of Appendix C, to very good approximation, we may regard all (non-gravastar) positive-pressure contributions as collisionless within the Friedmann source. Thus, the time-variation of ρ_0 comes

entirely from the time-variation of Δ_{BH} . The conservation Eqn. (12) then becomes

$$\frac{d\rho_s}{dt} + 3w_s H \rho_s = \frac{d\Delta_{\text{BH}}}{dt}. \quad (19)$$

Switching from coordinate time t to scale factor a gives

$$\frac{d\rho_s}{da} + 3w_s \frac{\rho_s}{a} = \frac{d\Delta_{\text{BH}}}{da}. \quad (20)$$

This equation can be separated with an integrating factor

$$\kappa(a, a_c) \equiv \exp\left(3 \int_{a_c}^a \frac{w_s(a')}{a'} da'\right) \quad (21)$$

$$= \frac{1}{a^3} \exp\left(3 \int_{a_c}^a \frac{\eta(a')}{a'} da'\right) \quad (22)$$

where we have defined the proportionality to be unity and a_c is a cutoff below which there are no gravastars. If we omit the cutoff parameter for κ , then we implicitly assume a_c . The resulting energy density is

$$\rho_s = \frac{1}{\kappa(a)} \int_0^a \frac{d\Delta_{\text{BH}}}{da'} \kappa(a') da', \quad (23)$$

where the lower-bound does not depend on a_c because Δ_{BH}/da vanishes by definition before a_c . When convenient, we will study the phenomenology of gravastars with the single parameter η held fixed. This is consistent with other phenomenological studies of gravastars. In practice, we will find that time-variation of η does not affect the essential cosmological signatures of a gravastar population.

3.1.1. Physical interpretation of DE

To develop some intuition for Eqn. (23), consider a sequence of instantaneous conversions

$$\frac{d\Delta_{\text{BH}}}{da} \equiv \sum_n Q_n \delta(a - a_n) \quad (24)$$

where Q_n is the comoving density of baryons instantaneously converted at a_n . Substitution into Eqn. (23) gives

$$\rho_s = \sum_n^{a_n \leq a} Q_n \frac{\kappa(a_n)}{\kappa(a)}. \quad (25)$$

Explicitly, at the instant of the m -th conversion a_m , we have the following comoving density of DE

$$\rho_s(a_m) = Q_m + \sum_n^{a_n < a_m} Q_n \frac{\kappa(a_n)}{\kappa(a_m)}. \quad (26)$$

Thus, at the instant of conversion, ρ_s agrees with a spatial average over the newly formed gravastars' interiors. In other words, a quantity of baryonic mass has been converted to an

equal quantity of DE. Beyond the instant of conversion, however, the contribution due to gravastars dilutes more slowly than the physical volume expansion. For example, in the de Sitter limit of $\eta \rightarrow 0$, we find that $\kappa \rightarrow a^{-3}$ and

$$\bar{\rho}_s(a) = \sum_n^{a_n \leq a} \frac{Q_n}{a_n^3} \quad (\eta \equiv 0). \quad (27)$$

In this case, the physical baryon density becomes ‘‘frozen in’’ at the time of conversion. To maintain locality in general, one might conclude that each gravastars' local mass Q_n must increase such that

$$Q_n \propto \kappa a^3, \quad (28)$$

but this would violate the Strong Equivalence Principle (e.g. Will 1993). Though such behavior is conceivable within scalar-tensor theories, we will remain focused on gravastars within GR.

Evidently, we cannot make any quantitative statements about the spatial location of the subsequent energy averaged to produce ρ_s . This is by choice, as our analysis is designed to minimize the impact of the unknown local details that produce the gravastar. Since we have accomplished this through covariant conservation of stress-energy, we can proceed with confidence that our predictions are entirely consistent within GR. Strictly speaking, however, Eqn. (17) must be interpreted as a motivation for η , and nothing more.

4. OBSERVATIONAL IMPLICATIONS

To begin constraining the gravastar hypothesis, we determine when gravastar production is observationally viable. Our discussion will proceed chronologically through the history of the Universe. This will inform our subsequent analysis: $\Omega_\Lambda^{\text{eff}}$ at late times will depend on an order-of-magnitude understanding of its early-time behavior.

4.1. Constraint on primordial pBH β as a function of temperature

The usual constraint on the fraction β of critical density capable of collapse into a primordial BH is expressed in terms of the mass of the target hole: $\beta(M)$ (e.g. Carr 2003). The mass of the hole is related to T via

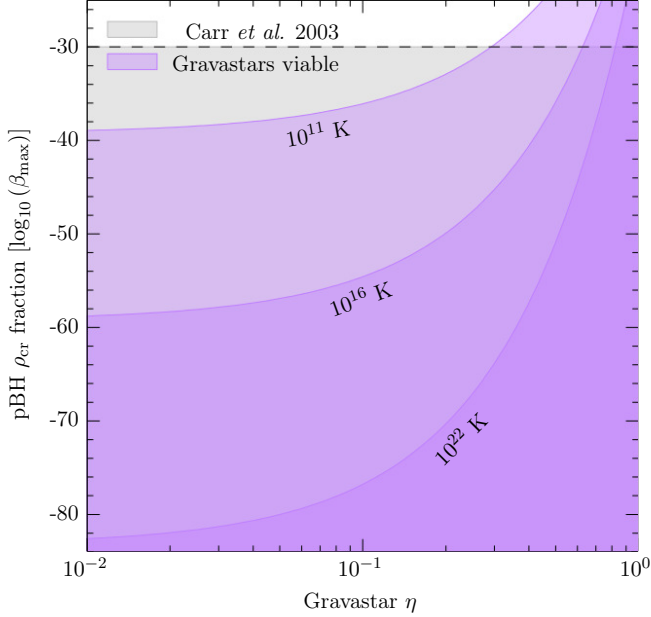
$$M(a) \simeq \frac{a^2}{2\sqrt{\Omega_r}} = \frac{1}{2\sqrt{\Omega_r}} \left(\frac{T_0}{T}\right)^2 \quad (29)$$

where Ω_r is the radiation density parameter today. Thus, we may construct an analogous constraint $\beta(T)$, where T is some temperature during the radiation-dominated epoch. We have switched to temperature using $a = T_0/T$, where $T_0 = 2.75\text{K}$ is the CMB temperature today.

Assume that all primordial BHs are produced at a single moment in time a_p

$$\frac{d\Delta_{\text{BH}}}{da} = \Omega_{\text{pBH}}(a) \delta(a - a_p). \quad (30)$$

Figure 1. Maximum fraction β of the critical density that can become primordial black holes as a function of gravastar crust parameter η . The constraint is determined by requiring the population-induced DE not exceed Ω_Λ . Increasing color (opacity) denotes increasing temperature of the formation epoch: $10^{22}K$ is the end of inflation and $10^{11}K$ is big bang nucleosynthesis. Formation is assumed to be instantaneous and monochromatic at the indicated epochs.



Here Ω_{pBH} is the comoving pBH density at a_p . For simplicity, consider η fixed in time. In this setting, Eqn. (21) becomes

$$\kappa = a^{-3(1-\eta)}. \quad (31)$$

Inserting this and Eqn. (30) into Eqn. (23) we find

$$\rho_s = \left(\frac{a}{a_p}\right)^{3(1-\eta)} \Omega_{\text{pBH}}(a_p), \quad (32)$$

and evaluating at the present day gives

$$\Omega_\Lambda \geq a_p^{3(\eta-1)} \Omega_{\text{pBH}}(a_p). \quad (33)$$

The present-day dark energy density gives a conservative upper bound because we are neglecting accretion. According to Carr (2003, Eqn. 7),

$$\Omega_{\text{pBH}}(a) = \frac{\beta \Omega_R}{a}, \quad (34)$$

which we can relate to Ω_m at the epoch of equality $\Omega_R = a_{\text{eq}} \Omega_m$. With these relations, Eqn. (33) becomes

$$\Omega_\Lambda \geq \frac{\Omega_m a_{\text{eq}} \beta}{a_p^{4-3\eta}}. \quad (35)$$

Rearranging the previous expression for β we find

$$\beta \leq \frac{\Omega_\Lambda a_p^{4-3\eta}}{\Omega_m a_{\text{eq}}} \approx a_p^{4-3\eta} \times 10^3, \quad (36)$$

which is presented in Figure 1.

Of course we do not claim that detection of even a single gravastar could enforce the constraints shown in Figure 1. The essential point, however, is that primordial production of gravastars is heavily disfavored. For small η , the amplification in energy density from the $a^{3\eta-4}$ term is extreme at primordial epochs.

4.2. Gravastars as the only source of dark energy

The prediction given in Eqn. (23) tightly correlates the dark energy density to the matter density. This suggests a natural resolution to the coincidence problem: gravastars are responsible for all of the cosmological dark energy. This possibility is plausible because the $\kappa(a, a_c) \approx a^{-3}$ in Eqn. (23) strongly amplifies the effect of conversion at early times. Unfortunately, until gravitational wave observatories begin to constrain Δ_{BH} , a precise discussion must remain focused on the late-time changes in $\Omega_\Lambda^{\text{eff}}$. To frame these changes in an appropriate context though, it is useful to understand the general features of any gravastar formation history that could suffice to resolve the coincidence problem. Since this is a very important consequence of a gravastar population, we will approach the question in two complementary ways.

4.2.1. Technique I: Instantaneous formation epoch from present-day BH density

First, we will determine an instantaneous formation epoch, given the present-day BH density. In other words, we will determine an instantaneous formation time a_f for all BH density such that the correct Ω_Λ is obtained. When gravitational wave observatories have constrained this density directly, this estimate can be checked anew. Until then, we will use the stellar population based BH model developed in Appendix E.

To proceed with an order of magnitude estimate, we again assume that all gravastars are produced at a single moment in time a_f

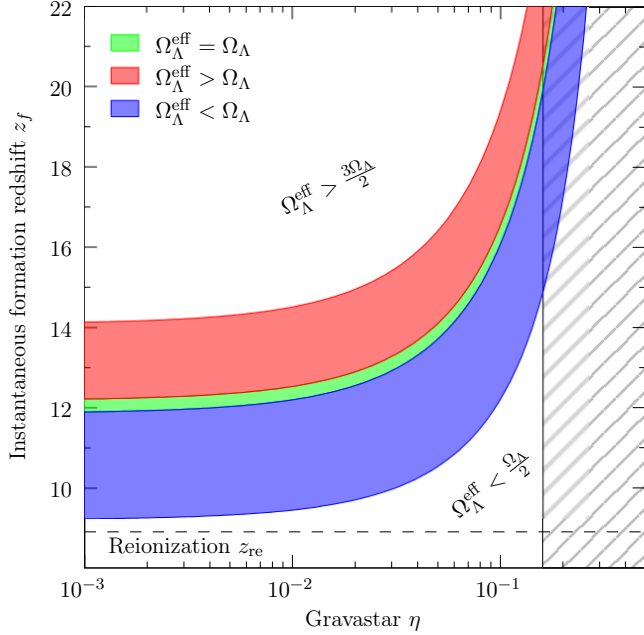
$$\frac{\Delta_{\text{BH}}}{da} = \Omega_{\text{BH}} \delta(a - a_f). \quad (37)$$

We take the total cosmological density in gravastars to be the present-day values

$$\Omega_{\text{BH}} \equiv \begin{cases} 3.02 \times 10^{-4} & \text{(rapid)} \\ 3.25 \times 10^{-4} & \text{(delayed)} \end{cases}. \quad (38)$$

Here, rapid and delayed refer to the stellar collapse model as detailed by Fryer et al. (2012). These values are likely slight underestimates due to accretion, which is neglected in Appendix E. Note that these values are consistent with the fraction of stars that collapse to BH, as estimated by Brown & Bethe (1994). Substituting the approximation Eqn. (37)

Figure 2. Estimated instantaneous gravastar formation redshift z_f , consistent with present day DE density. The horizontal axis gives the deviation η from a perfect de Sitter ($w_s = -1$) contribution to the cosmological source, due to the presence of gravastar crusts. Note that the onset of star formation $z_{\text{early}} \equiv 20$ encloses the viable region (green/light grey) for $\eta < 0.16$. The red (medium grey) region indicates Ω_Λ within a factor of 1.5 of the present day value, while the blue (dark grey) region indicates Ω_Λ within a factor of 0.5 of the present day value.



into Eqn. (23) we find

$$z_f = \left(\frac{\Omega_\Lambda}{\Omega_{\text{BH}}} \right)^{1/3(1-\eta)} - 1, \quad (39)$$

where we have again fixed η , and used that $\kappa(1, a_c) = 1$ for any fixed η . The instantaneous formation epoch is displayed in Figure 2.

4.2.2. Technique II: Constant formation from onset, rate consistent with γ -ray opacity

The stellar model used in §4.2.1 may suffer from systematics associated with interpolating the collapse remnant distributions between only two metallicities. To estimate the effect of this systematic, we will use unrelated astrophysical constraints determined from γ -ray opacity reported by Inoue et al. (2014). We will assume that a constant fraction of stellar density collapses to BH between stellar onset z_{early} up until some cutoff time z_f . We will determine the value of z_f such that the produced BH density yields the observed Ω_Λ today. We will further assume that the stellar density formation rate during $z_f < z < z_{\text{early}}$ is constant.

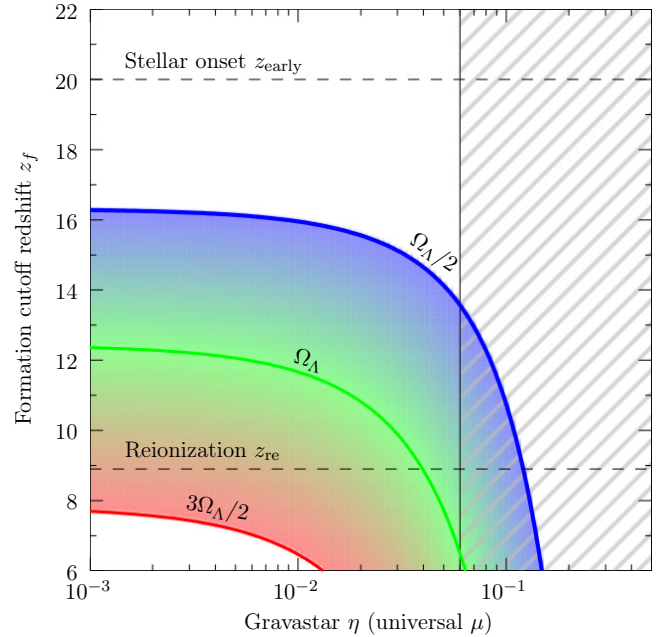
Since we are considering formation over an extended period of time, for simplicity, we continue to restrict our atten-

Table 1. Constraints on Population III star formation

Parameter	Value (natural units)	Reference
$d\rho_s/dt, z \sim 20$	$< 5.4 \times 10^{-2}$	Inoue et al. (2014, Fig. 2)
$d\rho_s/dt, z \sim 6$	$< 5.4 \times 10^{-3}$	Inoue et al. (2014, Fig. 2)
A	< 22.7	Abel et al. (2002)
Ξ	10^{-1}	Table 5

NOTE—data are used to constrain an approximate gravastar formation epoch, which suffices to produce all present-day dark energy density Ω_Λ by some cutoff redshift z_f . Variables defined in the text. The results of this analysis can be found in Figure 3.

Figure 3. Estimated dark energy density induced by gravastar formation from onset of stellar formation at $z_{\text{re}} \equiv 20$ until some cutoff z_f . This assumes a constant, but conservative, primordial rate of stellar density production $d\rho/dt \equiv 5.3 \times 10^{-3}$. This value is consistent with the more conservative γ -ray opacity constraints reported by Inoue et al. (2014) at $z \sim 6$ (see Table 1). Further assumptions include a fixed fraction of stellar density collapsing into BH and a constant amplification due to accretion. Note consistency with Figure 2, and convergence in the de Sitter limit $\eta \rightarrow 0$. Green (light grey) indicates production of the present-day Ω_Λ , red (medium grey) indicates excessive production up to $3\Omega_\Lambda/2$, and blue (dark grey) indicates insufficient production no less than $\Omega_\Lambda/2$.



tion to η fixed in time. Under these assumptions, we find that

$$\Omega_\Lambda = \int_{a_{\text{early}}}^{a_f} a^{-3(1-\eta)} A \Xi \frac{d\rho_g}{da} da. \quad (40)$$

Here we have introduced a constant collapse fraction Ξ and a factor A to account for accretion processes. We will take

$A \sim 10$. This is reasonable, given that Li et al. (2007) have shown that accretion can be very efficient at primordial times. With the constant star formation rate assumption, we may use the chain rule to write

$$\Omega_\Lambda = A\Xi \frac{d\rho_g}{dt} \int_{a_{\text{early}}}^{a_f} \frac{da}{Ha^{4-3\eta}}. \quad (41)$$

We present reasonable data for the above parameters in Table 1, where the formation rates listed are upper limits. Given the matter-dominated Hubble factor

$$H = \frac{\sqrt{\Omega_m}}{a^{3/2}}, \quad (42)$$

we may integrate Eqn. (41) and solve for the cutoff time. The result is

$$a_f = \left[\frac{3\Omega_\Lambda \sqrt{\Omega_m}}{A\Xi} \left(\frac{d\rho_g}{dt} \right)^{-1} \left(\eta - \frac{1}{2} \right) + a_{\text{early}}^{3(\eta-1/2)} \right]^{1/3(\eta-1/2)}. \quad (43)$$

The behavior of Eqn. (43), converted to redshift, is shown in Figure 3.

Note that we have taken the 10× more conservative bound established at $z \sim 6$. If we take $\Xi \sim 0.01$, there is no viable space. This is consistent with the stellar model of Appendix E, where the primordial collapse fraction is $\Xi \sim 0.1$. It is not surprising that the collapse remnant model's primordial Ξ is larger than the value of Brown & Bethe (1994), because their analysis depends on iron cores, which are not present in Population III stars. Note that the fraction of matter density converted to gravastar material under our assumptions,

$$\Omega_{\text{BH}} = A\Xi \frac{d\rho_g}{dt} \int_{a_{\text{early}}}^{a_f} \frac{da}{Ha} < 6.5 \times 10^{-4}, \quad (44)$$

is consistent with the present-day Ω_{BH} used in §4.2.1.

4.2.3. Discussion

In this section, we have considered whether gravastars alone could account for the present-day observed DE density. This is plausible because the DE induced by gravastar formation is amplified by $\sim 1/a^3$. Using two complementary techniques, we have estimated an approximate formation epoch for gravastars, which suffices to produce the present-day observed Ω_Λ . Encouragingly, both techniques agree that sufficient production is viable over a large range of η . This resolves the coincidence problem (e.g. Amendola & Tsujikawa 2010, §6.4) of a narrow permissible value for Ω_Λ . Furthermore, both techniques converge toward $z_f \sim 12$ and produce excluded regions for gravastar η

$$\eta \lesssim 1.6 \times 10^{-1} \quad (\text{instantaneous}) \quad (45)$$

$$\eta \lesssim 6.0 \times 10^{-2} \quad (\text{constant cutoff}). \quad (46)$$

Above these thresholds, resolution of the coincidence problem by gravastars is disfavored. As we will soon see, this exclusion is consistent with those based on late-time behavior and existing Planck constraint.

This result is very useful for many reasons. Most importantly, the viable region lies squarely in the middle of the epoch of primordial star formation. This suggests that a naturally emerging population of gravastars can produce the correct DE density. In addition, the density Ω_{BH} converted to induce this effect is $\sim 0.1\%$ of Ω_m . This is well within uncertainties on the Planck best-fit value for Ω_m . Since $z_f \ll z_{\text{CMB}}$, production of a sufficient population can occur without breaking agreement with precision CMB astronomy. In other words, CMB anisotropies are not altered at any level. Finally, gravastar formation at $z < 20$ can establish a present-day valued DE density after star formation has begun. Thus, initial conditions, and therefore results, of precision N -body simulations are not altered.

In any scenario where $\eta > 0$, the produced physical DE density will diminish with time $\propto 1/a^{3\eta}$. Relative to the required present day value of Ω_Λ then, the physical DE density is larger in the past. This behavior is not relevant for the present discussion, as it represents a minor increase in any physical DE density due to gravastars with viable η . During the dark ages, the matter density (dominated by dark matter) completely overwhelms any DE. This effect, however, is tracked in §4.3.

For the subsequent discussion, we interpret these estimates in the following way: *if* gravastars are to resolve the coincidence problem, we expect that most of the dark energy density will be established by stellar and accretion physics taking place during $5 < z < 20$.

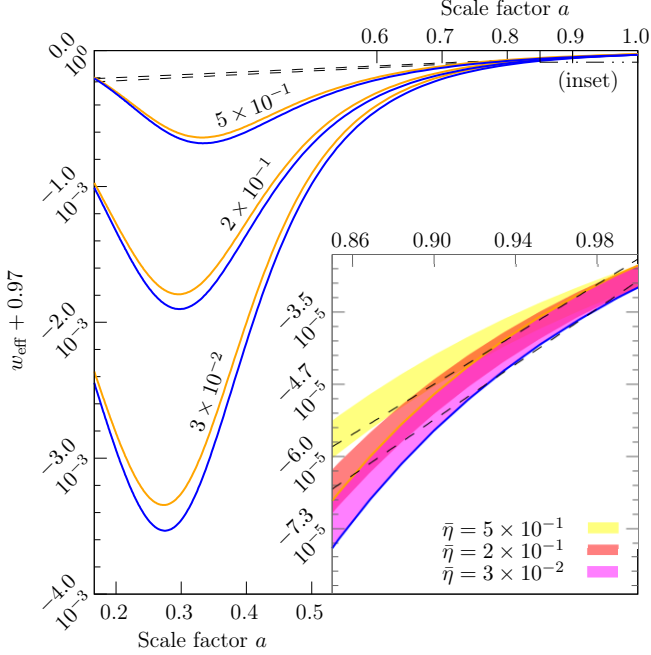
4.3. Gravastars analyzed in the dark fluid framework

Dark Energy is most commonly studied through constraint of three parameters: an energy density Ω_Λ , and the linear Taylor expansion, about $a \equiv 1$, of its equation of state parameter $w(a)$. This analysis of possible deviations from Λ CDM comes from the anticipated dynamics of a minimally coupled scalar field: the dynamics of an internally conserved fluid.

In the gravastar scenario, stellar collapse rates, subsequent accretion, and evolution in the stellar remnant distribution all induce changes in the DE density ρ_s . We can, however, choose to interpret this time-dependence of ρ_s as the dynamics of an internally conserved fluid. This leads to an effective equation of state parameter as follows. Define w_{eff} through

$$\frac{d\rho_s}{dt} \equiv -3w_{\text{eff}}H\rho_s. \quad (47)$$

Figure 4. Time-evolution of gravastar $w_{\text{eff}}(a)$ estimated from the stellar population. Both rapid (orange/light grey) and delayed (blue/dark grey) stellar collapse scenarios are shown. Best-fit lines (dashed) assuming the Planck linear ansatz near $a = 1$, shown for $\eta = 3 \times 10^{-2}$ only. Colors (greyscale) indicate distinct η (c.f. Figure 5). Note breakdown of the dark fluid (linear) approximation at $a = 0.9$.



Subtracting Eqn. (19) from Eqn. (47), switching to scale factor, substituting Eqn. (23), and solving for w_{eff} gives

$$w_{\text{eff}} = w_s - \frac{a \Delta'_{\text{BH}}}{3 \rho_s} \quad (48)$$

where prime denotes derivative with respect to a . Using the definition of κ in Eqn. (21) and linearity of the integral, we may re-express this relative to the present-day value of Ω_Λ

$$w_{\text{eff}} = w_s - \frac{d\Delta_{\text{BH}}}{da} \kappa(a, 1) \frac{a}{3} \left[\Omega_\Lambda - \int_a^1 \frac{d\Delta_{\text{BH}}}{da'} \kappa(a', 1) da' \right]^{-1}. \quad (49)$$

This form is advantageous as it samples only values very near to the present epoch, where constraint and systematics are well-characterized. The first-order Taylor expansion in $(1-a)$ of Eqn. (49) does not contain κ at all

$$w_{\text{eff}}^{(0)} = -1 + \left(\eta - \frac{\Delta'_{\text{BH}}}{3\Omega_\Lambda} \right) \Big|_{a=1} \quad (50)$$

$$w_{\text{eff}}^{(1)} = \frac{\Omega_\Lambda (\Delta''_{\text{BH}} - 2\Delta'_{\text{BH}}) - \Delta_{\text{BH}}'^2}{3\Omega_\Lambda^2} \Big|_{a=1} + \left(\frac{\eta \Delta'_{\text{BH}}}{\Omega_\Lambda} - \eta' \right) \Big|_{a=1}. \quad (51)$$

The coefficient Eqns. (50) and (51), combined with astrophysically measured values and uncertainties in BH popu-

lation parameters, will give a region which can be immediately compared against any Planck-style $w_0 - w_a$ constraint diagram.

The results of §4.2 suggest that most of Ω_Λ should be already produced by $z \sim 5$. In this case, we may approximate Eqn. (49) as

$$w_{\text{eff}} \simeq w_s - \Delta'_{\text{BH}} \kappa(a, 1) \frac{a}{3\Omega_\Lambda} \left[1 - \frac{\Delta'_{\text{BH}} \kappa(a, 1)}{\Omega_\Lambda} \right]. \quad (52)$$

We have shown that knowledge of the black hole mass function and the present-day dark energy density completely determines w_{eff} . In this way, gravitational wave observatory measurements of the BH population make definitive cosmological predictions. We already have a wealth of cosmological observations, however, with upcoming experiments (e.g. Levi et al. 2013, DESI) set to constrain w_{eff} . We may thus make predictions for gravitational wave observatories by inverting the above procedure. Solving for $d\Delta_{\text{BH}}/da$ by differentiating Eqn. (49) and re-integrating, we find

$$\frac{d\Delta_{\text{BH}}}{da} = 3\Omega_\Lambda \frac{w_s(a) - w_{\text{eff}}(a)}{a} \exp \left[3 \int_a^1 w_{\text{eff}}(a') \frac{da'}{a'} \right]. \quad (53)$$

Note that we have removed κ entirely through use of Eqn. (21). Given the particularly simple w_{eff} assumed by Planck

$$w_{\text{eff}}(a) \equiv w_0 + w_a(1 - a), \quad (54)$$

we may express Eqn. (53) in closed form

$$\frac{d\Delta_{\text{BH}}}{da} = 3\Omega_\Lambda [\eta - (1 + w_0 + w_a) + w_a a] \frac{\exp[3w_a(a-1)]}{a^{3(w_0+w_a)+1}}. \quad (55)$$

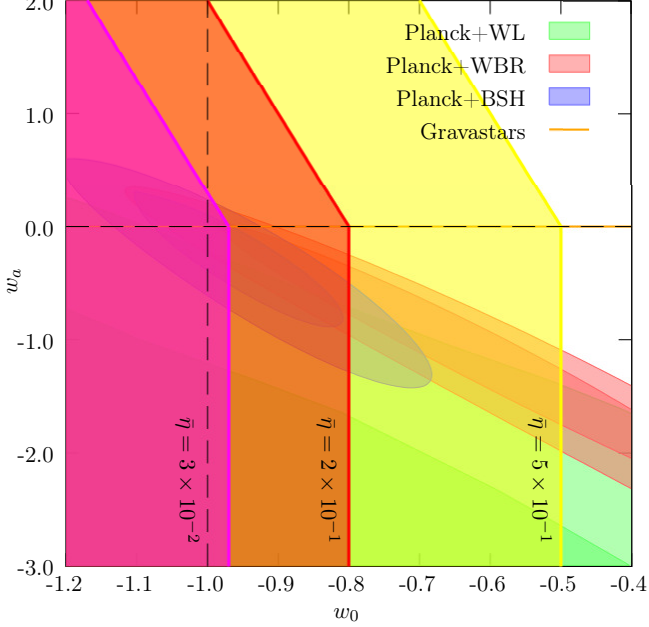
4.3.1. Estimation of w_{eff} from the comoving stellar density

In the gravastar scenario, the physical origin of DE is completely different than the internal dynamics of a scalar field. The linear model Eqn. (54), based on the dark fluid assumption, may not be the most suitable for characterization of a late-time gravastar DE contribution. In this section, we use a BH population model, developed from the stellar population in Appendix E, to investigate w_{eff} in the gravastar scenario. These results will allow us to estimate when Eqns. (54) and (55) well-approximate the time-evolution of the comoving BH density.

The BH population model of Appendix E does not account for accretion, so we must remain outside of any epoch where BH accretion is significant. Consistent with the simulations of Li et al. (2007), we consider only $z < 5$. To begin evaluation of Eqn. (49), we require $\kappa(a, 1)$, which requires η . For fixed η , the required integrations become trivial. We find

$$\kappa(a, 1) = \frac{1}{a^{3(1-\eta)}} \quad (56)$$

Figure 5. Gravastar constraint region (orange line/horizontal axis) estimated from the stellar population. Region is superimposed upon Planck constraints of the Dark Energy equation of state evolution. Overlaid “chevrons” represent positive BH density constraints for $a > 0.9$, which is the lower-bound a for validity of the Taylor expansion. Colors (greyscale) indicate distinct η (c.f. Figure 4). Chevron boundaries have thickness $\Delta'_{\text{BH}}(1)/3\Omega_\Lambda \sim 10^{-5}$. The intersection of these vertical bands with the horizontal band gives viable $w_0 - w_a$ for any particular η (c.f. Figure 6). Note that Planck+WBR is the Planck+WL+BAO/RSD combined constraint, where WL is weak lensing and BAO/RSD is baryon acoustic oscillations/redshift space distortions. BSH is a combined constraint from BAO, Type Ia Supernovae, and local measurements of the Hubble constant.



and predict for Eqn. (52)

$$w_{\text{eff}} \approx -1 + \eta - \frac{\Delta'_{\text{BH}}}{3\Omega_\Lambda a^{2-3\eta}} \left[1 - \frac{\Delta'_{\text{BH}}}{\Omega_\Lambda a^{3(\eta-1)}} \right]. \quad (57)$$

This relation is displayed in Figure 4. The range corresponds to “rapid” and “delayed” models of stellar collapse, as determined by Fryer et al. (2012). The collapse model determines the distribution of remnant masses, which evolves in time with metallicity. Given Δ_{BH} , Eqn. (57) provides a single parameter fit, with sub-percent precision, viable for $z < 5$. It is clear that the Planck linear ansatz is only useful for

$$a > 0.9 \quad z < 0.11 \quad (58)$$

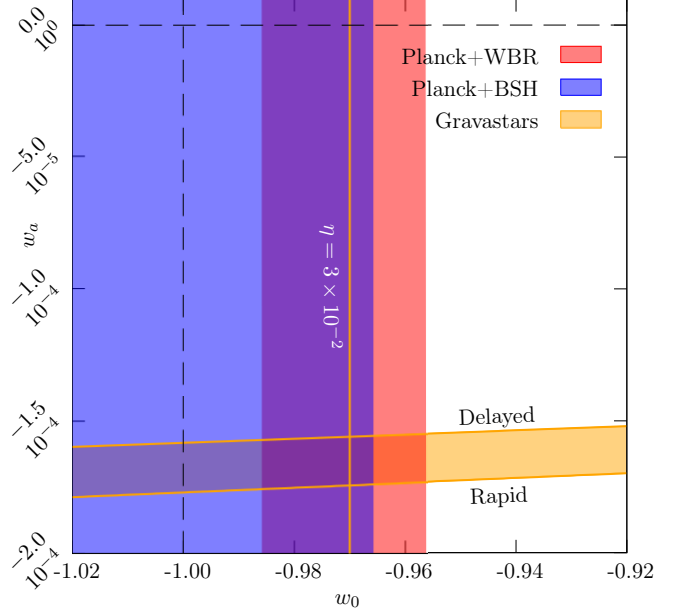
with departures growing significantly worse as $\eta \rightarrow 0$.

4.3.2. Planck and DES constraint of η at the present epoch

Physically, $d\Delta_{\text{BH}}/da \geq 0$ must be satisfied wherever ansatz Eqn. (54) is valid. From Eqn. (53), this constraint becomes an upper bound

$$w_{\text{eff}}^{(0)} \leq \eta(1) - 1. \quad (59)$$

Figure 6. Gravastar constraint region (orange/light grey) estimated from the stellar population, vertical axis magnified by 10^5 compared to Figure 5. The region is superimposed upon Planck constraints of the Dark Energy equation of state evolution. Stellar collapse model indicated via label. Acronyms are defined in the caption of Figure 5. Planck 2σ contours have been removed for clarity. For illustration, permissible region for $\eta \equiv 3 \times 10^{-2}$ shown, with thickness 10^5 smaller than indicated. The permissible region is the overlap of the orange band and the vertical orange line.



Regardless of any time-evolution in η , we may use Eqns. (50) and (51) to constrain η now. Eliminating η from these equations, we find a permissible line through $w_0 - w_a$ space

$$w_{\text{eff}}^{(1)} = \frac{\Delta'_{\text{BH}}}{\Omega_\Lambda} w_{\text{eff}}^{(0)} + \left(\frac{\Delta''_{\text{BH}} + \Delta'_{\text{BH}}}{3\Omega_\Lambda} - \eta'(1) \right). \quad (60)$$

We will use the BH population model, developed from the stellar population in Appendix E, to estimate the derivatives of Δ_{BH} . From Eqn. (E57), we numerically find that

$$\Delta'_{\text{BH}}(1) = \begin{cases} 5.364 \times 10^{-5} & \text{(rapid)} \\ 6.135 \times 10^{-5} & \text{(delayed)} \end{cases} \quad (61)$$

$$\Delta''_{\text{BH}}(1) = \begin{cases} -2.214 \times 10^{-4} & \text{(rapid)} \\ -2.447 \times 10^{-4} & \text{(delayed)} \end{cases}, \quad (62)$$

which will produce a permissible band in $w_0 - w_a$ space. For $\eta' \equiv 0$, this band is displayed in Figures 5 and 6. Evidently, Planck data disfavor gravastars with large η

$$0 < \eta(1) \leq 3 \times 10^{-2} \quad \eta'(1) \equiv 0. \quad (63)$$

Within this range, however, gravastars are consistent with Planck best fit constraints.

By inspection of Eqn. (60), η' simply translates the constraint region vertically. If we are to remain consistent with $d\Delta_{\text{BH}}/da \geq 0$ for $0.9 < a < 1$, we must have

$$w_{\text{eff}}^{(1)} \leq -10w_{\text{eff}}^{(0)} + 10[\eta(a) - 1]. \quad (64)$$

This bound, and the positivity bounds given in Eqn. (59) are displayed in Figure 5 for a variety of η .

Recent results constraining the w CDM model from the Dark Energy Survey (DES) (Abbott et al. 2017) cannot be immediately applied to constrain η . This is because w_{eff} induced by a gravastar population changes in time even if η remains fixed for all time. Since we predict only small changes in w_{eff} , however, it is reasonable to expect that the w CDM model will approximate the gravastar scenario at late times. Indeed, their reported value of w (Abbott et al. 2017, Eqn. VII.5) becomes the following constraint on η

$$\eta < 4 \times 10^{-2} \quad (w_0 = -1.00_{-0.05}^{+0.04}), \quad (65)$$

which is consistent with the constraints reported in §4.2.3.

5. CONCLUSION

Gravitational vacuum stars have become a viable and popular theoretical alternative to the pathological classical black hole (BH) solutions of GR. These objects appear as BHs to exterior vacuum observers, but contain de Sitter interiors beneath a thin crust. This crust is located above the classical Schwarzschild horizon, placing the entire gravastar in causal contact with the exterior universe. Many existing studies have focused on the observational consequences of the crust region for optical and gravitational wave signatures. These studies are hindered by systematics relating to the crust, which is only loosely constrained theoretically. In this paper, we have developed complementary constraints on the gravastar scenario based on the well-established properties of their de Sitter interiors.

We place our gravastars within a flat Friedmann cosmology, which is nowhere vacuum, and show from the action principle that the zero-order Friedmann source must contain an averaged term sensitive to the interiors. This is consistent with Birkhoff's theorem, which does not apply without vacuum boundaries. Through conservation of stress-energy, this term induces a time-dependent Dark Energy (DE) density. This density is directly correlated to the evolution of non-linear structure via star formation and subsequent collapse. The gravastar crust produces a small deviation η from a pure de Sitter ($w = -1$) equation of state. This deviation becomes the single parameter characterizing the gravastar population.

We replace all black holes with gravastars and consider the cosmological effects of their subsequent DE contribution at three epochs. During the primordial epoch ($T \sim 10^{22}\text{K} - T \sim$

10^{11}K), we find that the fraction of matter collapsing into a primordial gravastar population with $\eta < 10^{-1}$ is constrained between $\sim 10 - 50$ orders of magnitude more than existing primordial BH constraints. During the dark ages ($8.9 \lesssim z \lesssim 20$) we show, via two approaches, that existing astrophysical data support formation of a population of gravastars that can account for all of the present-day DE density. We show that any gravastar population with crust parameter $\eta < 6 \times 10^{-2}$ can resolve the coincidence problem. During late-times ($z < 5$), we precisely interpret the gravastar scenario in the usual language of a time-varying dark fluid. Using a BH population model built from the cosmic star formation history and stellar collapse simulations, we predict time-variation in the magnitude of $w(a)$ that tracks star formation. We demonstrate complete consistency with Planck, given a gravastar population with $\eta < 3 \times 10^{-2}$. Further, we predict very little time-variation in $w(a)$ at late times, consistent with the recent results of the Dark Energy Survey.

We make definitive predictions for both the gravitational astronomy community and dark energy surveys in the form of unexpected quantitative correlations between the time-evolution of the DE density and the BH population. In summary, the cosmological consequences of a gravastar population are unambiguous, readily testable, and already resolve many outstanding observational questions, without requiring any *ad hoc* departure from GR.

All code for generating the presented data and its visualizations is released publicly (opr4).

Software: opr4, scipy (Oliphant 2007), GNU Maxima, gnuplot

This paper is dedicated to the memory of Prof. J. M. J. Madey, inventor of the free-electron laser. His emphasis on the ‘‘paramount importance of boundary conditions’’ heavily influenced this research. The author thanks N. Kaiser (IfA) for sustained theoretical criticism, J. Weiner (U. Hawai‘i) for thorough technical feedback concerning the action, and T. Browder (U. Hawai‘i) and K. Nishimura (U. Hawai‘i) for copious feedback during the preparation of all versions of the manuscript. Additional thanks go to S. Ballmer (aLIGO) for conversations concerning the capabilities of present and planned gravitational wave observatories, C. Corti (AMS02) for visualization suggestions, C. McPartland (IfA) for guidance in the stellar literature, N. Warrington (U. Maryland) for stimulating discussions and feedback, J. Kuhn (IfA) for comments on rich clusters, J. Learned (U. Hawai‘i) for encouragement, R. Matsuda (U. Tokyo/IPMU) for comments on clarity, and The University of Tokyo for hospitality during the preparation of this manuscript. This work was performed with financial support from the Fulbright U.S. Student Program.

APPENDIX

A. ASSUMPTIONS OF THE *DE FACTO* FRIEDMANN SOURCE AT LATE-TIMES

In this appendix, we highlight non-trivial assumptions that enter the *de facto* Friedmann source (DFFS) during matter domination. In the DFFS, one imposes an additional hypothesis on the physical background matter density at late-times (Peebles 1980, §9, §97)

$$\bar{\rho}_b(t) \propto a^{-3}. \quad (\text{A1})$$

To understand its origin, consider the conservation of stress-energy statement for a single component perfect fluid

$$\frac{d}{dt} (\bar{\rho}_b a^3) = -3H\bar{\mathcal{P}}_b a^3. \quad (\text{A2})$$

Here H is the Hubble parameter (defined in §C.1) and $\bar{\mathcal{P}}_b \equiv T^{kk}$ is the background physical pressure. Equation (A1) then follows if one defines $\bar{\mathcal{P}}_b(t) \equiv 0$. Note that this is an assumption beyond Einstein's equations with the RW metric. The origin of this assumption is microphysical. For $20 \lesssim z \lesssim z_{\text{CMB}}$, mean free paths of all particles (even hypothetical dark matter) are very large; particles are not scattering into or out of comoving volumes. This fixes the comoving number density of particles. Since the rest masses of elementary particles do not change, it follows that $\bar{\mathcal{P}}_b$ must be zero.

Given the lack of a formal mathematical definition for the DFFS, we consider the operational definition of the perturbations to $\bar{\rho}_b(t)$, given by Peebles (1980, §81). He states that “we can imagine that observers spread through the universe and moving with the matter keep a record of the local density as a function of proper time, $\bar{\rho}(\mathbf{x}, t)$. As the observers come within the horizon, their records can be acquired and compared.” We now paraphrase this operational procedure:

1. Each observer measures and broadcasts (e.g. via light signals with presumably the same frequency) their own local density $\bar{\rho}(\mathbf{x}, t)$.
2. Each observer receives the others' broadcasts and averages them with his own to produce a background $\bar{\rho}_b(t)$.
3. Each observer computes his density perturbation as $\bar{\rho} - \bar{\rho}_b$.

The same procedure may be performed with the local pressure $\bar{\mathcal{P}}(\mathbf{x}, t)$, which will be non-zero in general. Between $20 \lesssim z < z_{\text{CMB}}$, averaged pressures remain negligible compared to averaged energy densities. Below $z \lesssim 20$, however, collapsed structures begin to form.

In order to justify continued use of the homogeneous and isotropic fluid ansatz for $z \lesssim 20$, one redefines Peebles' observers. One regards an observer as reporting on a very large volume containing many gravitationally bound systems. Next, one invokes any number of formal embedding solutions to GR (e.g. Einstein & Straus 1945), which glue a Schwarzschild metric into a RW metric. The existence of such formal solutions motivates defining a spatially isolated system to contribute only an active gravitational mass to the averaged energy density T^{00} . In this setting, the only pressures that could contribute to T^{kk} would be from large structures, like rich clusters. As we show in Appendix F, however, upper bound pressures for these systems are $\mathcal{P} \lesssim 10^{-5}\rho$. Thus, it may seem completely justifiable to continue to regard $\bar{\mathcal{P}}_b \equiv 0$.

It must be emphasized, however, that formal embedding solutions are logically distinct from the perturbative treatment. The perturbative treatment assumes instead the exact RW background. Suppose we were unable to redefine our observers, and consider a Peebles' type observer within the core of a gravastar. Here the pressure is equal in magnitude, but opposite in sign, to the energy density. The DFFS discards these contributions. In other words, the DFFS defines $\bar{\mathcal{P}}_b \equiv 0$ for $z < 20$ because this is consistent with Newtonian intuition and static strong gravity in asymptotically flat space.

B. THE SPATIALLY AVERAGED NATURE OF THE FRIEDMANN SOURCE

In this Appendix, we rederive Friedmann's equations directly from the Einstein-Hilbert action. The action is a manifestly global quantity, from which local equations of motion are constructed. Since the action is an integral statement over the space-time manifold, it will allow us to cleanly reconcile the isotropy and homogeneity of the RW metric ansatz with the anisotropic distribution of actual stress-energy.

Our approach will be to rewrite Friedmann's isotropic and homogeneous model as a scalar theory in flat-space. The result will be an unambiguous interpretation of the Friedmann source as the flat-space, comoving coordinate average of the trace of the

stress-tensor. This well-motivated notion of “locality” within the Friedmann model is lost if one begins with Einstein’s equations under the RW ansatz, simply because one must invoke some *ad hoc* procedure (e.g. Appendix A) to produce an isotropic and homogeneous source from the actual stress-energy.

The principle of stationary action requires that the total action S be stable, at first order, to variations in the dynamical degrees of freedom

$$\delta S \equiv \delta(S_M + S_G) \equiv 0 \quad (\text{B3})$$

where S_M represents the matter action and S_G represents the gravitational action. We will consider the canonical definition of the stress-energy tensor $\bar{T}_{\mu\nu}$ given by Weinberg (1972, §12.2)

$$\delta S_M \equiv -\frac{1}{2} \int_{\mathcal{M}} \bar{T}_{\mu\nu} \delta \bar{g}^{\mu\nu} \sqrt{-\bar{g}} \, d^4x. \quad (\text{B4})$$

Here \mathcal{M} denotes the smooth manifold associated with the metric $\bar{g}_{\mu\nu}$ (O’neill 1983, §3.2), $\delta \bar{g}^{\mu\nu}$ is the variation of the inverse metric, and $\sqrt{-\bar{g}}$ is the metric determinant. Recall that an overset bar denotes a physical quantity, as opposed to a comoving one. For the gravitational action S_G , consider the usual Einstein-Hilbert action

$$S_G \equiv \frac{1}{16\pi G} \int_{\mathcal{M}} \bar{R} \sqrt{-\bar{g}} \, d^4x. \quad (\text{B5})$$

Here \bar{R} is the Ricci scalar determined from the Levi-Civita connection compatible with $\bar{g}_{\mu\nu}$, and we are using MKS units with $c \equiv 1$.

In comoving coordinates, the RW metric takes the form of Eqn. (C31). Defining the conformal time η through

$$dt \equiv a(\eta) \, d\eta, \quad (\text{B6})$$

Eqn. (C31) becomes

$$ds^2 = a^2 \left(-d\eta^2 + d\mathbf{x}^2 \right). \quad (\text{B7})$$

Note that Eqn. (B7) takes the form of a conformal transformation of flat spacetime

$$\bar{g}_{\mu\nu} = a(\eta)^2 \eta_{\mu\nu} \quad (\text{B8})$$

where $\eta_{\mu\nu}$ is the Minkowski metric of special relativity. We may thus express \bar{R} in the conformally flat frame (Wald 2010, §D)

$$\bar{R} = a^{-2} R - 2(n-1) \eta^{\mu\nu} a^{-3} \nabla_\mu \nabla_\nu a \quad (n \equiv 4) \quad (\text{B9})$$

$$= -6 \eta^{\mu\nu} a^{-3} \partial_\mu \partial_\nu a. \quad (\text{B10})$$

with regular partial derivatives. Similarly, the metric determinant in the conformally flat frame becomes

$$\sqrt{-\bar{g}} = a^4. \quad (\text{B11})$$

The gravitational action then becomes

$$S_G = -\frac{6}{16\pi G} \int_{\mathcal{M}} a \eta^{\mu\nu} \partial_\mu \partial_\nu a \, d^4x \quad (\text{B12})$$

and its variation with respect to the single physical degree of freedom $a(\eta)$ is

$$\delta S_G = -\frac{3}{4\pi G} \int_{\mathcal{M}} \delta a \partial^\mu \partial_\mu a \, d^4x \quad (\text{B13})$$

where we have discarded the boundary term.

To find δS_M , we start with the most general fluid stress-tensor, which applies to any type of matter and coordinate choice. It is given by Hu (2004, Eqn. 6) as

$$\bar{T}_\nu^\rho \equiv \begin{bmatrix} -\bar{\rho} & \bar{v}_i \\ \bar{u}^j & \bar{\pi}_i^j \end{bmatrix} (\eta, \mathbf{x}). \quad (\text{B14})$$

where \bar{v}^i and \bar{u}^i are future-directed timelike vector fields. We have eliminated the purely formal separation of background from perturbation for clarity. Now, we may lower an index in the usual way

$$\bar{T}_{\mu\nu} = \bar{T}_\nu^\rho \bar{g}_{\rho\mu}. \quad (\text{B15})$$

and use the chain rule to write

$$\delta\bar{g}^{\mu\nu} = -2a^{-3}\eta^{\mu\nu}\delta a. \quad (\text{B16})$$

Substitution of Eqns. (B8), (B11), (B14), and (B15) into Eqn. (B4) then gives

$$\delta S_M = \int_{\mathcal{M}} a^3 (-\bar{\rho} + \bar{\pi}_1^1 + \bar{\pi}_2^2 + \bar{\pi}_3^3) \delta a \, d^4x. \quad (\text{B17})$$

We may compress this further by defining the following notation

$$\bar{\mathcal{P}}(\eta, \mathbf{x}) \equiv \frac{1}{3} \sum_{i=1}^3 \bar{\pi}_i^i(\eta, \mathbf{x}) \quad (\text{B18})$$

to arrive at the desired expression

$$\delta S_M = \int_{\mathcal{M}} a^3 (-\bar{\rho} + 3\bar{\mathcal{P}}) \delta a \, d^4x. \quad (\text{B19})$$

We may now make explicit our claim that the Friedmann source is a spatial-slice average. Under the constraints of isotropy and homogeneity, δa can only be a function of η . This is because the variation must be consistent with the constraints imposed on the system under study (e.g. [Lanczos 2012](#)). We may thus expand the iterated integral of Eqn. (B19)

$$\delta S_M = \int a^3 \delta a \int_{\mathcal{V}} [-\bar{\rho}(\eta, \mathbf{x}) + 3\bar{\mathcal{P}}(\eta, \mathbf{x})] \, d^3\mathbf{x} \, d\eta \quad (\text{B20})$$

$$= \int a^3 \delta a \mathcal{V} \langle -\bar{\rho} + 3\bar{\mathcal{P}} \rangle \, d\eta \quad (\text{B21})$$

where \mathcal{V} is some fiducial spatial volume. Consider a typical arbitrary variation without symmetry requirements, i.e. $\delta g_{\mu\nu}(\eta, \mathbf{x})$. Since the variation is arbitrary, one is free to consider variations with compact spatiotemporal support. In such a case, the integrals appearing in the action and its variation can always be regarded as finite. In the RW setting, however, we are not free to enforce compact spatial support for $\delta a(\eta)$. This means that \mathcal{V} is infinite, and convergence issues might arise from an iterated integral representation (i.e. Fubini's theorem). This can be remedied by regarding \mathcal{V} as resulting from an arbitrary spatial cutoff for the integration domain. One then verifies that the result is independent of the cutoff.

Indeed, substitution of Eqns. (B13) and (B21) into Eqn. (B3) gives

$$\int \delta a \left\{ \frac{d^2 a}{d\eta^2} - \frac{4\pi G}{3} a^3 \langle \bar{\rho} - 3\bar{\mathcal{P}} \rangle \right\} \, d\eta = 0 \quad (\text{B22})$$

where the fiducial spatial volume successfully divides off. The resulting field equation

$$\frac{d^2 a}{d\eta^2} = \frac{4\pi G}{3} a^3 \langle \bar{\rho} - 3\bar{\mathcal{P}} \rangle \quad (\text{B23})$$

agrees with the standard Eqns. (C32) and (C33) summed and shifted to conformal time. Note that, in the standard scenario, all $\bar{\pi}_i^i$ are equal, and so $\bar{\mathcal{P}}$ is the usual isotropic pressure. The advantage of working directly from the action is that the spatial average of the source is made manifest. This is the main result of this appendix.

B.1. Discussion

The spatial average of Eqn. (B23) is entirely consistent with the operational definition given by [Peebles \(1980, §81\)](#). The temporary appearance of the spatial volume \mathcal{V} is interesting. Einstein's equations are "local" in the sense of "localized in space." This leads to the intuition that all dynamical fields are position-dependent. In the context of cosmology, this is reinforced from

the Newtonian approximation, where $a(\eta, \mathbf{x})$ defines a coordinate change (e.g. Peebles 1980), which can vary from point to point. Together, these predispositions have sometimes (e.g. Rácz et al. 2017) led to the perception that there is some sort of local scale factor $a(\eta, \mathbf{x})$, which the Friedmann model somehow digests into $a(\eta)$.

One can decompose Eqn. (B19) into a sum of N open, disjoint, spacelike regions and average over these

$$\delta S_M = \sum_{m \in \mathcal{M}}^N \int a^3 \delta a \mathcal{V}_m \langle -\bar{\rho} + 3\bar{\mathcal{P}} \rangle_m d\eta. \quad (\text{B24})$$

Here, the cutoff procedure discussed previously is equivalent to requiring $N < \infty$. Until \mathcal{V}_m is large enough for a given epoch, these averages will not be equal and so the equations of motion will not be well-defined. This clarifies $\mathcal{V}^{1/3}$ as the lower bound length-scale implicit to the isotropic perfect fluid model (Landau & Lifshitz 1959, §1). The novelty within cosmology is that this length-scale is, in general and practice, time-dependent. Technically, one should not assume the same perfect fluid model throughout the entire history of the universe.

C. CONSISTENCY OF DFFS- Λ CDM AND CFS- Λ CDM

In this Appendix, we demonstrate that Λ CDM with the CFS remains observationally viable. As established in §4.2 and discussed in Appendix A, there is no need to track pressures until the non-linear growth regime. Before this regime, therefore, the DFFS and the CFS are equivalent. Once into the non-linear regime, predictions are not made with linear perturbation theory. Instead, N -body simulations with initial conditions determined by linear perturbation theory are required. We thus show that the standard Newtonian behaviour on an expanding background is observationally unchanged. To do this, we show that the ‘‘Hubble drag’’ and density contrast are observationally equivalent in the DFFS and the CFS.

Our approach in this section will be to conservatively bound the influence of pressures from typical systems on both cosmological and peculiar motions. We will quantify the influence on cosmological motion with the fractional difference in the Hubble rate

$$\frac{\Delta H}{H} \equiv \frac{H_{\Lambda\text{CDM}} - H_{\text{test}}}{H_{\Lambda\text{CDM}}}. \quad (\text{C25})$$

We will quantify the influence on peculiar motions with the difference in total comoving energy densities

$$\Delta q \equiv q_{\Lambda\text{CDM}} - q_{\text{test}}. \quad (\text{C26})$$

Here q is defined in Eqn. (C34) as the total density appearing in the Friedmann energy Eqn. (C32). We will use DFFS- Λ CDM (with purely collisionless matter) as the reference expansion, and consider only Planck best-fit cosmological parameters for Ω_m and Ω_Λ (Planck Collaboration et al. 2016).

To build an extremely conservative upper bound on the effect of pressures neglected in the DFFS, we consider the densest stars, the neutron stars. While the neutron star equation of state is an active area of research, example stable polytrope models (e.g. Hansen et al. 2012) give a local core pressure of $\bar{\mathcal{P}} \sim 10^{-6}\bar{\rho}$. For simplicity, we will regard the equation of state parameter w_s as constant during the following analysis.

We define a depletion fraction by dividing the cosmic stellar density, given in derivative form in Eqn. (E68), by Ω_m . We then numerically integrate Eqn. (C38). We choose extremely conservative (i.e. large) values for the equation of state parameter

$$10^{-4} < w_s < 1. \quad (\text{C27})$$

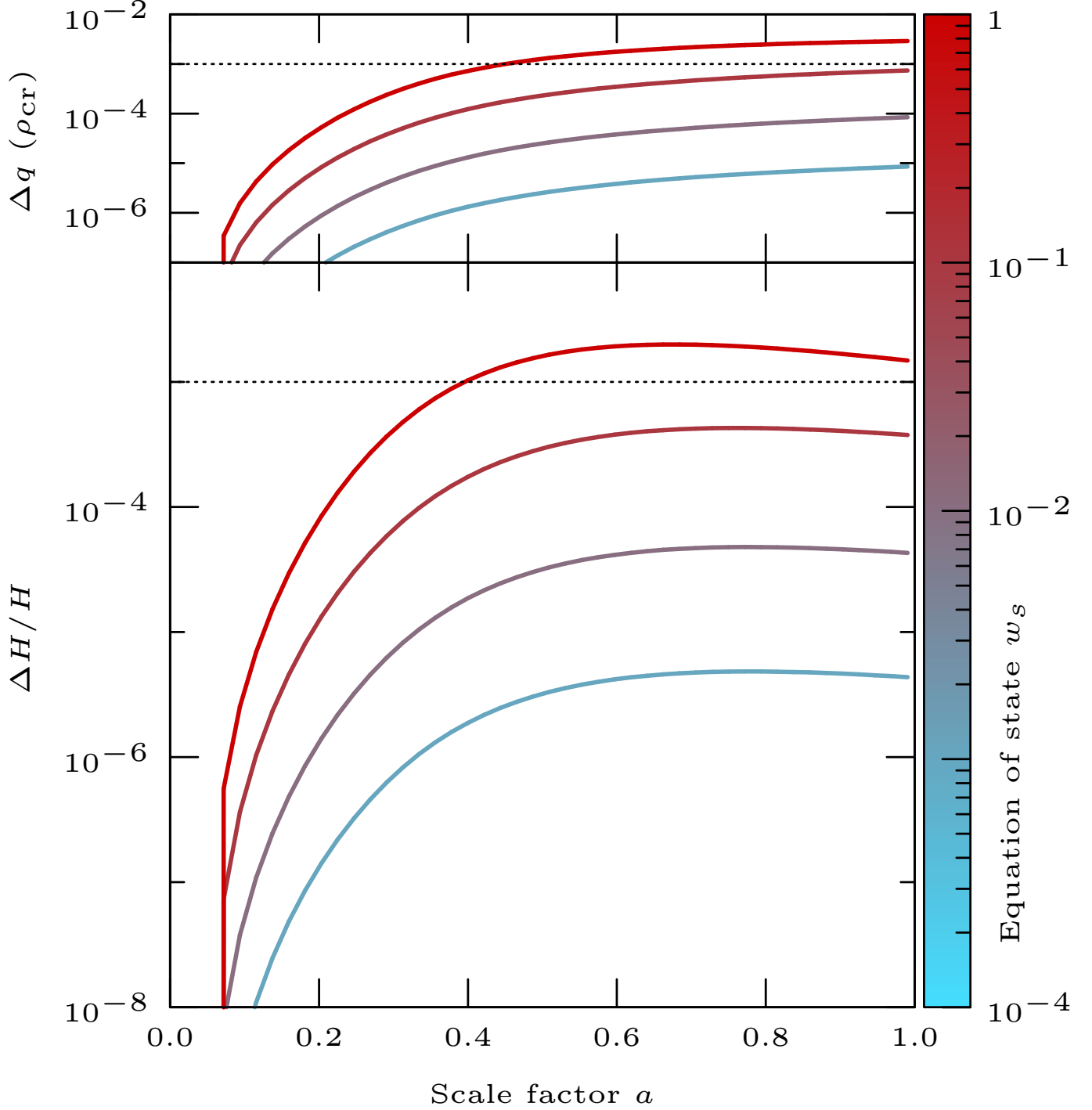
The results for the expansion history are shown in the bottom panel of Figure 7. It is clear that keeping positive pressures in the CFS cannot observably alter cosmological motions.

From Eqn. (C25) and Figure 7, the expansion loses energy relative to the DFFS with fixed comoving densities. From conservation of energy and momentum given in Eqn. (12),

$$\frac{d\rho_s}{dt} + \frac{d\rho_0}{dt} = -3Hw_s\rho_s, \quad (\text{C28})$$

it is clear that ρ_s can only remain constant at fixed w_s when $d\rho_0/dt \propto H$. Therefore, a small amount of energy density Δq is subsequently lost after the conversion of collisionless stress ρ_0 to stress under compression ρ_s . This loss, relative to the DFFS, is

Figure 7. Cosmological quantities in the CFS, relative to the DFFS, if the stellar population contributes with $\mathcal{P}_s \equiv w_s \rho_s$. Pressures $\mathcal{P}_s \lesssim 10^{-4} \rho_s$ are conservative (i.e. very large) for gravitationally bound systems at late times. Stellar growth follows [Madau & Dickinson \(2014\)](#). The palette gives the equation of state parameter w_s . As can be seen, the CFS is observationally indistinguishable from Λ CDM. (Top panel) Difference in comoving energy density relative to the DFFS. The dotted horizontal line gives an observational upper bound for present day values. (Bottom panel) Fractional difference of expansion history relative to the DFFS. The dotted horizontal line gives an observational upper bound for present day values.



shown in the top panel of Fig. 7. To understand the influence of this loss, recall that peculiar motions are sourced by the energy

density contrast (Peebles 1980, §7)

$$\nabla^2 \phi = \frac{3}{2} \left[\bar{\rho}(\mathbf{x}, a) - \frac{q(a)}{a^3} \right] a^2. \quad (\text{C29})$$

Here $\bar{\rho}(\mathbf{x}, a)$ is the total local density, ϕ is the Newtonian gravitational potential, and q is the (background) comoving energy density defined in Eqn. (C34). In bound systems at late times,

$$\bar{\rho}(\mathbf{x}, a) \gg \frac{q(a)}{a^3} \gg \frac{\Delta q(a)}{a^3}. \quad (\text{C30})$$

It is immediately clear that Δq can have no observable effect on the local dynamics of any contemporary system.

In summary, we have demonstrated that even conservative (i.e. large) estimates of pressure contributions to the CFS produce no observable discrepancies from the pressure-free DFFS. This is true both for cosmological motions, as characterized by H , and for peculiar motions as determined by the density contrast. These results establish that the CFS is observationally consistent with the DFFS under the assumptions of Λ CDM.

C.1. Friedmann's equations

Here we derive the form of Friedmann's equations used in our numerical analysis. Units will remain explicit until Eqn. (C38), which is written with the units used elsewhere in this paper. We begin with the spatially flat Robertson-Walker line element

$$g_{\mu\nu} = -dt^2 + a(t)^2 d\mathbf{x}^2 \quad (\text{C31})$$

with $a(t)$ dimensionless. Substitution of Eqns. (9), (10), and (C31) into Einstein's equations with cosmological constant term Λ gives the Friedmann equations

$$H^2 = \frac{\gamma^2}{a^3} \left[\rho_0(a) + \rho_s(a) + \frac{\Lambda}{3\gamma^2} a^3 \right] \quad (\text{C32})$$

$$H^2 + 2\frac{\ddot{a}}{a} = -\frac{3\gamma^2}{a^3} \left[\mathcal{P}_s(a) - \frac{\Lambda}{3\gamma^2} a^3 \right] \quad (\text{C33})$$

where dot denotes derivative with respect to coordinate time. Here $H = \dot{a}/a$ and $\gamma^2 \equiv 8\pi G/3$. Define the total comoving energy density q , effective equation of state w_s , and scale velocity v by

$$q \equiv \rho_0(a) + \rho_s(a) + \frac{\Lambda}{3\gamma^2} a^3 \quad (\text{C34})$$

$$P_s \equiv w_s \rho_s(a) \quad (\text{C35})$$

$$v \equiv \frac{da}{dt}. \quad (\text{C36})$$

Substitution of Eqns. (C34) and (C36) into Eqn. (C32) gives an algebraic constraint

$$v^2 = \frac{q}{a}. \quad (\text{C37})$$

Substitution of Eqns. (11), (C35), and (C37) into Eqn. (C33) gives a single dynamical equation, which we express in terms of a

$$\frac{dv}{da} = \frac{3a\Omega_\Lambda}{2v}(1 + w_s) + \frac{3w_s\Omega_m}{2va^2}(1 - \Delta(a)) - \frac{v}{2a}(3w_s + 1). \quad (\text{C38})$$

The dynamics described by Eqn. (C38) are completely general.

D. CAUSALITY WITHIN THE CFS

In this Appendix, we discuss causality in the perturbative expansion about a RW background, given the CFS defined in Appendix B. GR possesses a well-posed initial value formulation (e.g. Wald 2010, §10). In other words, starting from reasonable

initial data, the metric and stress-energy evolve uniquely and causally. For regular (non-singular) perturbations (e.g. [Lin & Segel 1988](#), §7.1), one expands the relevant dynamical quantities in a perturbation series

$$g_{\mu\nu} \equiv \sum_{n=0}^{\infty} g_{\mu\nu}^{(n)} \quad (\text{D39})$$

$$T_{\mu\nu} \equiv \sum_{n=0}^{\infty} T_{\mu\nu}^{(n)}. \quad (\text{D40})$$

Since the dynamical equations of GR are non-linear, it is not true that each term in the expansion must evolve causally. Only the converged series are subject to this constraint.

Consider the formation of a single gravastar, described in a perturbation series with the (0)-order metric defined to be RW. As detailed in [Appendix B](#), the transition of baryonic matter into vacuum will change the (0)-order source. This change is, by definition, acausal since the (0)-order source contains no position dependence. By construction of the first-order theory, the linearized (1)-order perturbations (on top of any background) propagate causally. If there are acausal features in the (0)-order solution, it must be that the higher order perturbations act to restore the causal character of the entire converged series. We do not attempt a general proof of this statement, but use the DE problem, and previous attempts at its resolution within GR, to provide plausibility for the above assertion.

[Buchert & Räsänen \(2012\)](#) review arguments that the higher-order terms in the perturbative treatment mimic DE through “backreaction.” [Ishibashi & Wald \(2005\)](#), however, argued years earlier that this effect is far too small. What piques our attention, however, is that [Räsänen \(2004, §3\)](#) found that the effect is of the wrong sign. In fact, this is consistent with the gauge invariant findings of [Abramo et al. \(1997\)](#), who report a negative backreaction at primordial times.

Given our developed gravastar context, we speculate that the role of backreaction is to transiently cancel the imprint of newly formed gravastars from the (0)-order source. Note that this effect is localized in spacetime. This is because stars are collapsing to gravastars everywhere, and so there is a mean separation between progenitors that is small compared to the horizon.

E. BH POPULATION ESTIMATION FROM THE STELLAR POPULATION

In this Appendix, we develop a relation between the stellar population and the BH population. This relation is not required to experimentally test the predictions of this paper. The only relevant observable Δ_{BH} will soon be constrained directly through gravitational wave astronomy. Relation to the stellar population, however, is natural since BHs come from stars. Further, a quantitative model will allow us to check consistency over a diverse set of existing astrophysical data. We will formally outline the procedure, and then construct a usable model.

Denote the comoving coordinate number density of galaxies with mass in the range dM_g by

$$\frac{dn_g}{dM_g} dM_g \quad (\text{E41})$$

Denote the *number count* of BHs with mass in the range dM_{BH} in a galaxy of mass M_g as

$$\frac{dN_{\text{BH}}(M_g, M_{\text{BH}})}{dM_{\text{BH}}} dM_{\text{BH}}. \quad (\text{E42})$$

We re-express this relation in terms of stars. Following [Fryer & Kalogera \(2001\)](#), we use the fact that BHs are sampled from the same distribution as stars to write

$$\frac{dN_{\text{BH}}}{dM_{\text{BH}}} = \frac{dN_*}{dM_*} \frac{dM_*}{dM_{\text{BH}}}. \quad (\text{E43})$$

Assembling Eqns. (E41), (E42), and (E43), the number count of BHs with mass in the range dM_{BH} across galaxies in the mass range dM_g is

$$\frac{dn_g}{dM_g} \frac{dN_*}{dM_*}(M_g, M_*) \frac{dM_*}{dM_{\text{BH}}} dM_{\text{BH}} dM_g. \quad (\text{E44})$$

To form a population average comoving coordinate density over some observable $X(M_{\text{BH}})$, we multiply by the observable and integrate over all *BH* masses and galaxy masses

$$\langle X \rangle \equiv \int_{m_g}^{\infty} \frac{dn_g}{dM_g} \int_{m_{\text{BH}}}^{\infty} X(M_{\text{BH}}) \frac{dN_*}{dM_*}(M_g, M_*) \frac{dM_*}{dM_{\text{BH}}} dM_{\text{BH}} dM_g. \quad (\text{E45})$$

Table 2. Astrophysical parameters for BH population estimation

Parameter	Value	Units	Reference
α	-2.35	-	Salpeter (1955)
R	0.27	-	Madau & Dickinson (2014)
m_c	0.1	M_\odot	Chabrier (2003)
m_{TOV}	3	M_\odot	Kalogera & Baym (1996)

Note that accretion effects do not change the number of objects, but that mergers do. Mergers also affect the total mass through radiative losses, which can be around 5% of the final remnant (e.g. Abbott et al. 2016). In the interest of simplicity, we do not attempt to take account of these effects.

To produce a quantitatively useful model from Eqn. (E45), we note that

$$\int_{m_c}^{\infty} \frac{dN_*(M_g, M_*)}{dM_*} M_* dM_* \equiv (1 - R)M_g \quad (\text{E46})$$

where R is the fraction of stellar mass returned to the host galaxy upon star death. Note that m_c is a cutoff mass for the stellar distribution. We next assume a power-law for this distribution

$$\frac{dN_*(M_g, M_*)}{dM_*} \equiv BM_*^\alpha \quad (\text{E47})$$

with the normalization B determined by Eqn. (E46). The result is

$$\frac{dN_*(M_g, M_*)}{dM_*} = -(2 + \alpha) \frac{M_g(1 - R)}{m_c^{\alpha+2}} M_*^\alpha. \quad (\text{E48})$$

Since Chabrier (2003) finds a flattening of the stellar IMF around $0.1M_\odot$, we will take

$$m_c \equiv 0.1M_\odot \quad (\text{E49})$$

to maintain the validity of our power-law assumption. Reasonable values for R and α are given in Table 2. Inserting Eqn. (E48) into Eqn. (E45) and integrating over the host galaxy masses, we find

$$\langle X \rangle = -\rho_g(a)(1 - R) \frac{(2 + \alpha)}{m_c^{\alpha+2}} \int_{m_{\text{BH}}}^{\infty} X(M_{\text{BH}}) M_*^\alpha \frac{dM_*}{dM_{\text{BH}}} dM_{\text{BH}} \quad (\text{E50})$$

where $\rho_g(a)$ is the comoving stellar density (e.g. Madau & Dickinson 2014, Fig. 11). To proceed further, we require $M_{\text{BH}}(M_*)$. This has been recently estimated through stellar collapse simulations by Fryer et al. (2012, Fig. 4). We consider a linear ansatz for simplicity

$$M_{\text{BH}}(M_*) \equiv kM_* - |b| \quad (\text{E51})$$

and give the fit parameters in Table 3. For ansatz Eqn. (E51), $b < 0$ and $k > 0$ are the only physically allowed values.

The most important case for our concerns is

$$X(M_{\text{BH}}) \equiv M_{\text{BH}}^q \quad q \in \mathbb{Q}. \quad (\text{E52})$$

For example, $q = 1$ will estimate the cosmological ρ_{BH} . Substituting Eqn. (E51) into Eqn. (E50), we find

$$\langle M_{\text{BH}}^q \rangle = -\rho_g(a)(1 - R) \frac{(2 + \alpha)}{m_c^{\alpha+2}} \int_{m_*}^{\infty} (kM_* - |b|)^q M_*^\alpha dM_* \quad (\text{E53})$$

Table 3. Linear fits to $M_{\text{BH}}(M_*)$

Metallicity	Model	Slope k	y-Intercept $ b (M_\odot)$	χ^2_ν
$Z = Z_\odot$	rapid	0.19 ± 0.06	0.038 ± 1.8	9.2
	delayed	0.23 ± 0.03	1.1 ± 0.96	2.3
$Z = 0$	rapid	1.2 ± 0.15	18 ± 3.7	34
	delayed	1.2 ± 0.22	18 ± 5.3	70

NOTE—parameters characterize a coarse fit $M_{\text{BH}} = kM_* - |b|$ to $M_{\text{BH}}(M_*)$ based on the stellar collapse simulations of Fryer & Kalogera (2001)

Table 4. Metallicity dependence of remnant population parameters

Parameter	Model	Normalization B	z -constant ζ
k	rapid	0.19	0.09
	delayed	0.23	0.083
$ b $	rapid	0.038	0.31
	delayed	1.11	0.14
m_*	Eqn. (E54)	11	0.01

NOTE—Fits are exponential $B \exp(\zeta z)$, assuming $Z(z = 20) \equiv 0$ (i.e. neglecting primordial metal abundances)

where we have switched to integration over the progenitors. In the relevant simulations of Fryer et al. (2012), the lower bound for the progenitors is $11M_\odot$. For our purposes, we will demand that the remnant object exceed the Tolman-Oppenheimer-Volkoff limit m_{TOV} for neutron-degeneracy pressure supported systems. Inspection of Fryer et al. (2012, Fig. 4) gives the following reasonable cutoffs

$$m_* = \begin{cases} 11M_\odot & Z = Z_\odot \\ 16M_\odot & Z = 0 \end{cases} \quad (\text{E54})$$

where Z is the stellar metallicity. Note that

$$m_0 \equiv |b|/k \quad (\text{E55})$$

gives the natural cutoff for our linear ansatz. This cutoff is aphysical because it corresponds to a massless remnant, but is theoretically useful to estimate systematics from Eqn. (E54).

E.1. Determining k , $|b|$, and m_* as functions of redshift

Since Fryer et al. (2012) only provide two metallicities, unfortunately we must interpolate the time-evolution of k , $|b|$, and m_* between only two points in time. From Madau & Dickinson (2014, Fig. 14), $Z(z)$ is reasonably well-approximated by an exponential. The simplest assumption is that k , $|b|$, and m_* are also exponentials

$$\{k, |b|, m_*\}(z) \equiv \{B\} \exp(\{\zeta\}z). \quad (\text{E56})$$

Here $\{B\}$ are the normalizations and $\{\zeta\}$ are redshift “time constants.” We present these fit parameters in Table 4 to k , $|b|$, and m_* for both rapid and delayed supernovae models.

Table 5. Fraction of comoving stellar density collapsed into BH, based on metallicity and supernovae engine

Metallicity	Model	$m_0 (M_\odot)$	$\Xi(m_*) (\%)$	$\Xi(m_0) (\%)$
$Z = Z_\odot$	rapid	0.15	2.6	$4 (m_{\text{TOV}})$
	delayed	4.8	2.8	3.2
$Z = 0$	rapid	15.7	11	11
	delayed	15.2	12	11

NOTE—Astrophysical parameters used are given in Table 2. For comparison, [Brown & Bethe \(1994\)](#) predict a late-time ($Z \sim Z_\odot$) collapse fraction $\Xi \sim 1\%$.

A more rigorous analysis would consider a range of monotonic interpolations to determine the systematic error introduced in all subsequent quantities involving k , $|b|$, and m_* . We forgo this procedure since a single additional $M_{\text{rem}}(M_{\text{prog}})(Z)$ for $Z \in (0, Z_\odot)$ would mitigate this necessity.

E.2. Cosmological BH density

The $q = 1$ case corresponds to the cosmological comoving coordinate BH mass density. Usefully, $q = 1$ can be integrated by hand in closed form

$$\rho_{\text{BH}}(a) = (1 - R) \left[k \left(\frac{m_*}{m_c} \right)^{\alpha+2} - \frac{|b|}{m_c} \left(\frac{\alpha+2}{\alpha+1} \right) \left(\frac{m_*}{m_c} \right)^{\alpha+1} \right] \rho_g(a) \quad (\text{E57})$$

$$\equiv \Xi(a) \rho_g(a) \quad (\text{E58})$$

where we have defined the collapse fraction $\Xi(a)$. Time variation in Ξ can come from α , k , $|b|$, and m_* . For the collapse models detailed in Table 3, we give cutoff parameters and collapse fractions in Table 5, based on the astrophysical parameters given in Table 2. We make no effort to propagate errors due to the coarseness of the fit.

To quantify the sensitivity of these data to the cutoffs given in Eqn. (E54), note that the integrand remains finite for $q = 1$. Thus, we may naturally remove the cutoff and set $m_* \equiv m_0$. We have done this except where $m_0 < m_{\text{TOV}}$, where we take $m_* \equiv m_{\text{TOV}}$. In all cases, the solar metallicity results are consistent with $\Xi \sim 1\%$ as computed by [Brown & Bethe \(1994\)](#) via entirely different means.

We have assumed zero time lag between the stellar population and the BH population. Let us justify this simplification for $0.2 \ll z < 20$. This places us within matter domination, so we may approximate

$$H \simeq \frac{\sqrt{\Omega_m}}{a^{3/2}}. \quad (\text{E59})$$

Considering the differentials, we see that

$$da = \frac{\sqrt{\Omega_m}}{a^{1/2}} dt \quad (\text{E60})$$

and so we may approximate the lag in scale a_L relative to the lag in time τ_L as

$$a_L \simeq \frac{\sqrt{\Omega_m}}{a^{1/2}} \tau_L. \quad (\text{E61})$$

According to dimensional arguments, for stars massive enough to collapse to BH, $\tau_L \lesssim 10^7$ years at metallicity Z_\odot . Given our choice in time unit, this becomes the upper bound

$$\tau_L \lesssim \frac{6 \times 10^{14} \text{ s}}{5 \times 10^{17} \text{ s}} \sim 10^{-3}. \quad (\text{E62})$$

Table 6. Adopted astrophysical parameters

Quantity	Value	Units	Reference
G	6.67×10^{-11}	$\text{m}^3 \text{kg}^{-1} \text{s}^{-2}$	Patrignani et al. (2016)
c	3.00×10^8	m s^{-1}	Patrignani et al. (2016)
M_\odot	1.99×10^{30}	kg	Patrignani et al. (2016)
H_0	69.3	$\text{km s}^{-1} \text{Mpc}^{-1}$	Planck Collaboration et al. (2016)
$M_\odot \text{Mpc}^{-3} \text{yr}^{-1}$	0.277	$\rho_{\text{cr}} H_0$	-

NOTE—Values used to construct unit conversions between $H_0 = \rho_{\text{cr}} \equiv 1$ and common literature units.

Note that this is a conservative upper bound on primordial star lifetimes. To justify the neglect of the time lag, we must have that

$$\rho_g(a - a_L(a)) = \rho_g[a(1 - a_L/a)] \simeq \rho_g(a) \quad (\text{E63})$$

and so we require that $a_L/a \ll 1$. A sufficient condition is then

$$\frac{a_L}{a} < \frac{\sqrt{\Omega_m}}{a^{3/2}} 10^{-3} \ll 1, \quad (\text{E64})$$

which implies

$$z \ll 148. \quad (\text{E65})$$

For representative numbers, at $z = 20$ the time lag is a 5% correction, but at $z = 5$ the time lag is a 0.8% correction. Most importantly, at the peak of star formation near $z \sim 2$, the time lag is a 0.2% correction. We may thus consider

$$\rho_{\text{BH}}(a) = \Xi(a)\rho_g(a) \quad (z < 5) \quad (\text{E66})$$

to good precision.

In practice, we will be interested in the late-time behavior of these quantities. Since ρ_{BH} depends on the entire conversion history, neglecting accretion could have a substantial effect on ρ_{BH} . Since Li et al. (2007) find that accretion effects diminish significantly below $z < 5$, it is more convenient to examine $d\rho_{\text{BH}}/da$

$$\frac{d\rho_{\text{BH}}}{da} = -\Xi(a)\frac{d\rho_g}{dz}\frac{1}{a^2} + \frac{d\Xi}{da}\rho_g. \quad (\text{E67})$$

A global fit, performed by Madau & Dickinson (2014), to very many stellar surveys gives the comoving stellar density as

$$\frac{d\rho_g}{dz} = 0.277 \frac{(R-1)\psi}{(1+z)H} \quad (\text{E68})$$

$$\psi \equiv 0.015 \frac{(1+z)^{2.7}}{1 + [(1+z)/2.9]^{5.6}} \quad (\text{E69})$$

$$R \equiv 0.27. \quad (\text{E70})$$

The factor of 0.277 converts units as listed in Table 6. We determine H given the Planck assumed dark energy equation of state Eqn. (54)

$$H(z) \equiv \sqrt{\Omega_m(1+z)^3 + \Omega_\Lambda(1+z)^{3[1+w_{\text{eff}}(0)]} \exp\left(-\frac{3w_a z}{z+1}\right)}. \quad (\text{E71})$$

E.3. Expectation values with generic q

It is useful to define notation to compress and de-dimensionalize

$$\lambda(q) = q + \alpha + 1 \quad (\text{E72})$$

$$r \equiv m_0/m_*. \quad (\text{E73})$$

We may now write the de-dimensionalized Eqn. (E53)

$$\langle M_{\text{BH}}^q \rangle = \rho_g(a)(R-1) \frac{(2+\alpha)|b|^{\lambda(q)}}{m_c^{\alpha+2} k^{\alpha+1}} \int_{1/r}^{\infty} (z-1)^q z^\alpha dz. \quad (\text{E74})$$

Notice that $z \geq 1$ always, and so the integrand remains real for all $q, \alpha \in \mathbb{R}$. We then perform an inversion $z \rightarrow 1/x$ to make the domain of integration finite

$$\langle M_{\text{BH}}^q \rangle = \rho_g(a)(R-1) \frac{(2+\alpha)|b|^{\lambda(q)}}{m_c^{\alpha+2} k^{\alpha+1}} \int_0^r (1-x)^q x^{-\lambda(q)-1} dx. \quad (\text{E75})$$

Define the following notation

$${}_2F_1\{q\} \equiv {}_2F_1(-q, -\lambda(q); -(q+\alpha); r). \quad (\text{E76})$$

We may then write

$$\int_0^r (1-x)^q x^{-\lambda(q)-1} dx = -\frac{{}_2F_1\{q\}}{\lambda(q)} r^{-\lambda(q)} \quad (\text{E77})$$

and finally we find

$$\langle M_{\text{BH}}^q \rangle = \rho_g(a)(1-R) \frac{(2+\alpha)m_*^{\lambda(q)} k^q} {m_c^{\alpha+2}} \frac{{}_2F_1\{q\}}{\lambda(q)}. \quad (\text{E78})$$

Values for ${}_2F_1\{q\}$ can be computed in any modern CAS.

F. SYSTEMS WITH LARGE VELOCITY DISPERSION

We wish to compute an order of magnitude pressure contribution from large, virialized systems, like rich clusters. Pressure supported clusters are regarded as ideal gases

$$\mathcal{P}_c = nkT \quad (\text{F79})$$

where \mathcal{P}_c is the pressure, n is the number density, k is Boltzmann's constant, and T is the temperature. Let m be a typical mass, then

$$\mathcal{P}_c = \frac{\rho_c kT}{m}. \quad (\text{F80})$$

Assuming a monoatomic gas, the average energy is

$$E = \frac{3}{2}kT. \quad (\text{F81})$$

One can construct a Newtonian kinetic energy from the velocity dispersion σ

$$E = \frac{1}{2}m\sigma^2. \quad (\text{F82})$$

Combining Eqns. (F81) and (F82) gives the temperature

$$kT = \frac{m\sigma^2}{3}. \quad (\text{F83})$$

To determine a reasonable upper bound, rich clusters can have $\sigma \sim 10^3$ km/s (Struble & Rood 1999). Since we work in natural units, $\sigma^2 \rightarrow (\sigma/c)^2 \sim 10^{-5}$. Thus, the kinetic pressure of a rich cluster goes as

$$\mathcal{P}_c \lesssim \frac{10^{-5}}{3} \rho_c. \quad (\text{F84})$$

REFERENCES

- Abel, T., Bryan, G. L., & Norman, M. L. 2002, *Science*, 295, 93
- Abramo, L. R. W., Brandenberger, R. H., & Mukhanov, V. F. 1997, *Physical Review D*, 56, 3248
- Ade, P., Aghanim, N., Arnaud, M., et al. 2016, *Astronomy & Astrophysics*, 594, A14
- Almheiri, A., Marolf, D., Polchinski, J., & Sully, J. 2013, *Journal of High Energy Physics*, 2013, 62
- Amendola, L., & Tsujikawa, S. 2010, *Dark Energy: Theory and Observations* (Cambridge University Press)
- Bhagwat, S., Brown, D. A., & Ballmer, S. W. 2016, *Physical Review D*, 94, 084024
- . 2017, *Physical Review D*, 95, 069906
- Broderick, A. E., & Narayan, R. 2007, *Classical and Quantum Gravity*, 24, 659
- Brown, G. E., & Bethe, H. A. 1994, *ApJ*, 423, 659
- Buchert, T., & Räsänen, S. 2012, *Annual Review of Nuclear and Particle Science*, 62, 57
- Carr, B. 2003, *Quantum Gravity*, 301
- Chabrier, G. 2003, *Publications of the Astronomical Society of the Pacific*, 115, 763
- Chapline, G. 2003, *International Journal of Modern Physics A*, 18, 3587
- Chirenti, C., & Rezzolla, L. 2016, *Physical Review D*, 94, 084016
- Chirenti, C. B., & Rezzolla, L. 2007, *Classical and Quantum Gravity*, 24, 4191
- . 2008, *Physical Review D*, 78, 084011
- DeBenedictis, A., Horvat, D., Ilijić, S., Kloster, S., & Viswanathan, K. 2006, *Classical and Quantum Gravity*, 23, 2303
- Dwyer, S., Sigg, D., Ballmer, S. W., et al. 2015, *Physical Review D*, 91, 082001
- Dymnikova, I. 1992, *General relativity and gravitation*, 24, 235
- Einstein, A., & Straus, E. G. 1945, *Rev. Mod. Phys.*, 17, 120
- Fryer, C. L., Belczynski, K., Wiktorowicz, G., et al. 2012, *The Astrophysical Journal*, 749, 91
- Fryer, C. L., & Kalogera, V. 2001, *The Astrophysical Journal*, 554, 548
- Gliner, E. B. 1966, *Soviet Journal of Experimental and Theoretical Physics*, 22, 378
- Hansen, C. J., Kawaler, S. D., & Trimble, V. 2012, *Stellar interiors: physical principles, structure, and evolution* (Springer Science & Business Media)
- Harko, T., Kovács, Z., & Lobo, F. S. 2009, *Classical and Quantum Gravity*, 26, 215006
- Hu, W. 2004, arXiv preprint astro-ph/0402060
- Inoue, Y., Tanaka, Y. T., Madejski, G. M., & Domínguez, A. 2014, *The Astrophysical Journal Letters*, 781, L35
- Ishibashi, A., & Wald, R. M. 2005, *Classical and Quantum Gravity*, 23, 235
- Kalogera, V., & Baym, G. 1996, *The Astrophysical Journal Letters*, 470, L61
- Lanczos, C. 2012, *The variational principles of mechanics* (Courier Corporation)
- Landau, L. D., & Lifshitz, E. M. 1959, *Fluid mechanics* (Oxford: Pergamon Press)
- Levi, M., Bebek, C., Beers, T., et al. 2013, arXiv preprint arXiv:1308.0847
- Li, Y., Hernquist, L., Robertson, B., et al. 2007, *ApJ*, 665, 187
- Lin, C.-C., & Segel, L. A. 1988, *Mathematics applied to deterministic problems in the natural sciences* (SIAM)
- Lobo, F. S. 2006, *Classical and Quantum Gravity*, 23, 1525
- Madau, P., & Dickinson, M. 2014, *Annual Review of Astronomy and Astrophysics*, 52, 415
- Maggio, E., Pani, P., & Ferrari, V. 2017, arXiv preprint arXiv:1703.03696
- Martin-Moruno, P., Garcia, N. M., Lobo, F. S., & Visser, M. 2012, *Journal of Cosmology and Astroparticle Physics*, 2012, 034
- Mazur, P. O., & Mottola, E. 2004, *Proceedings of the National Academy of Sciences of the United States of America*, 101, 9545
- Oliphant, T. E. 2007, *Computing in Science Engineering*, 9, 10
- O’neill, B. 1983, *Semi-Riemannian geometry with applications to relativity*, Vol. 103 (Academic press)
- Patrignani, C., Richardson, P., Zenin, O., et al. 2016, *Chin. Phys. C*, 40, 100001
- Peebles, P. J. E. 1980, *The large-scale structure of the universe* (Princeton university press)
- Planck Collaboration, Ade, P. A. R., Aghanim, N., et al. 2016, *A&A*, 594, A13
- Rács, G., Dobos, L., Beck, R., Szapudi, I., & Csabai, I. 2017, *Monthly Notices of the Royal Astronomical Society: Letters*, 469, L1
- Räsänen, S. 2004, *Journal of Cosmology and Astroparticle Physics*, 2004, 003
- Sakai, N., Saida, H., & Tamaki, T. 2014, *Physical Review D*, 90, 104013
- Salpeter, E. E. 1955, *The Astrophysical Journal*, 121, 161
- Struble, M. F., & Rood, H. J. 1999, *The Astrophysical Journal Supplement Series*, 125, 35
- Uchikata, N., & Yoshida, S. 2015, *Classical and Quantum Gravity*, 33, 025005
- Visser, M., & Wiltshire, D. L. 2004, *Classical and Quantum Gravity*, 21, 1135
- Wald, R. M. 2010, *General relativity* (University of Chicago press)
- Weinberg, S. 1972, *Gravitation and cosmology: principles and applications of the general theory of relativity*, Vol. 67 (Wiley New York)
- Will, C. M. 1993, *Theory and Experiment in Gravitational Physics* (Cambridge University Press)
- Yunes, N., Yagi, K., & Pretorius, F. 2016, *Physical Review D*, 94, 084002